The Cretaceous of the Cameroon Atlantic Basin (Central Africa): Sediment provenance, correlation, paleoenvironment and paleogeographic evolution of the Eastern Proto-Atlantic margin (Central Gondwana)

Milan Stafford Tchouatcha (inter_milanac@yahoo.fr)
Arnaud Patrice Kouske
Wael Fathi Galal
Magdy Salah Mahmoud
Christel Sobdjou Kemteu
Leopold Darlus Ngantchu
Justeol Pholker Takou
Alain Préat
Cyrile Gastel Noubissie
Valerie Therese Ngonlep Miyemeck
Pierre Ricard Njike Ngaha

Research Article

Keywords: Sediment origin, Sedimentation environment, Correlation, Paleogeographic evolution, Atlantic Basin, Cameroon.

Posted Date: June 23rd, 2022

DOI: https://doi.org/10.21203/rs.3.rs-1748977/v1

Additional Declarations: No competing interests reported.

Version of Record: A version of this preprint was published at Environmental Earth Sciences on February 9th, 2023. See the published version at https://doi.org/10.1007/s12665-023-10765-x.

Abstract

An integration of geochemistry, mineralogical and palynological data is used to depict the sediment provenance and distribution, the sedimentary environment and the paleogeographic evolution of the Cretaceous Atlantic Basin of Cameroon. The basin is located along the African western coast, in the heart of the Guinea Gulf, and includes the Campo, Douala, and Rio-del-Rey sub-basins from South to North. The sediments of the Campo sub-basin are derived from rocks of intermediate composition, those of the Douala sub-basin from intermediate to mafic rocks in the southern and felsic rocks in the northern parts, and those of the Rio-del-Rey sub-basin from felsic rocks with a contribution of rocks of intermediate composition. The paleoweathering index and Index of Chemical Variability values, ranging respectively from 71.26 to 76.88 and 0.98 to 2.12, 67.15 to 99.39 and 0.37 to 0.90 and 73.17 to 92.90 and 0.44 to 10.03 respectively for Campo, Douala and Rio-del-Rey sub-basins, indicate sub-maturity, high maturity and sub- to high maturity, respectively, of the Campo, Douala and Rio-del-Rey deposits. Al_2O_3 vs. V and Al_2O_3 vs. P_2O_5 plots, and palynologic data such as marine (e.g. dinoflagellates and microforaminifera and continental species (e.g. *Classopollis* sp., *Ephedripites* sp., *Botryococcus* sp.) suggest a deposition in more or less deep lacustrine (Campo sub-basin), fluvio-deltaic to shallow marine (Douala sub-basin), and marginal to shallow marine (Rio-del-Rey sub-basin) environments. Chemical Index of Alteration, X-Ray diffraction and palynologic data point to arid to semi-arid, semi-arid and arid to semi-arid conditions, respectively in the Campo, Douala and Rio-del-Rey sub-basins. The tectonic setting diagram suggests collision tectonic events that are inconsistent with the classic geological history of the Atlantic Basin. The situation is in fact related to Precambrian events that affected the basement rocks from which the studied sediments were derived, and probably to the compressional tectonics during the evolution of the South Atlantic Ocean. Although these sub-basins share the same geological history, there are some differences, such as the degree of sediment maturity, the diagenetic effects, the lithology of rock sources, the paleoenvironments of deposition and their fluctuation, depending on the moment the tectonic of Atlantic opening reached them (northward progression of the W-E extension) and the northern shearing along the southern area of the Benue through axis (Rio-del-Rey). The geological history of the Cameroon Atlantic Basin is similar to those of Gabonese and Nigerian basins, along the African western coast, and of those of the Brazilian basins along the eastern coast (Santos Basin to Pernambuco-Paraiba Basin)

1. Introduction

The history of the Atlantic Basin is related to the breaking up of the Gondwana continent initiated during the Late Jurassic-Early Cretaceous transition with the opening of the South Atlantic Ocean between the South American and African plates (Boltenhagen 1976; Salard-Cheboldaeff 1978; Maurin and Guiraud 1993; Edet and Nyong 1994; Pletsh et al. 2001; Chen et al. 2013; Njike Ngaha et al. 2014), the Central Atlantic (Scotese 2001; Afenzar and Essamoud 2018; Dowla et al. 2018) and the North Atlantic (Alves and Cunha 2018). Many studies of the Western African Margin, e.g. Cameroon margin (Nguene et al. 1992; Ntamak-Nida et al. 2008, 2010; Njike Ngaha et al. 2014; Njoh and Taku 2016; Njoh et al. 2018), the Nigerian margin (Adediran et al. 1991; Boboye and Okon 2014; Madukwe 2019) and the East Brazilian margin (Koutsoukos et al. 1991; Karner and Driscoll 1999; Carvalho et al. 2006) revealed the common history of these margins. A similar Cretaceous magmatism has also been reported in both sides of the South Atlantic (Goode et al. 2018; Kurobasa et al. 2018). The Cameroon Atlantic Basin which resulted from this geodynamic activity during Early Cretaceous times (Fig. 1) comprises three sub-basins, from south to north, the Campo, the Douala, and the Rio del Rey sub-basins.

The Campo sub-basin typically consists of Cretaceous deposits, while the Douala (Nkenfack et al. 2012; Mbesse et al. 2012; Njike and Eno Belinga 1987; Njike Ngaha et al. 2014) and Rio-del-Rey (Njoh et al. 2018) sub-basins are composed of Cenozoic fillings, in addition to Cretaceous deposits.

These Cretaceous sub-basins have been the subject of several palynological and biostratigraphic studies, by Belmonte (1966), Chevalier (1982), Njike Ngaha and Eno Belinga (1987) and Ntamak-Nida et al. (2008) in the Aptian-Albian Campo sub-basin; by Salard-Cheboldaeff (1977, 1978, 1979, 1981) in the Maastrichtian, Njoh et al. (2014) in the Albian-Turonian, Njike Ngaha et al. (1987), Njike Ngaha et al. (2014) in the Cenomanian-Turonian of the Douala sub-basin and by Njoh et al. (2013a,b, 2018) in the Albian-Maastrichtian of the Rio-del-Rey sub-basin;

The Cretaceous deposits are very diversified. In the Campo and Rio-del-Rey sub-basins they consist of varied coarse- and fine-grained materials suggesting diversified sedimentation conditions and origins (Njike Ngaha and Eno Belinga 1987, Ntamak-Nida et al. 2008, 2010, for the Campo area and Njoh et al. 2013a, b, 2016, 2018 for Rio-del-Rey area). Sediment distribution and provenance have been carried out in the Atlantic Basin both from sedimentology (Douala sub-basin, e.g. Njike Ngaha 1984; Njike Ngaha and Eno Belinga 1987; Tchouatcha et al. 2021a), Rio-del-Rey sub-basin (Njoh and taku 2016; Njoh et al. 2018) and Campo sub-basin (Ntamak-Nida et al. 2008, 2010) and geochemistry (Douala sub-basin, e.g. Ngueutchoua et al. 2017, 2019a, b, Esue et al. 2021; Tchouatcha et al. 2021a) and Campo sub-basin (Ashukem et al. 2022). Despite these numerous studies, it appears that, sedimentation conditions and sediment provenance derived from geochemistry of fine-grained sediments in the Campo and Rio-del-Rey sub-basins and parts of the Douala sub-basin are still lacking, as stratigraphic correlation between the sub-basins and other basins on both sides of the Atlantic Ocean.

For a better understanding of the Cameroon coastal basins, a reliable correlation between the three sub-basins is needed. In this study, we use geochemical and mineralogical signatures of fine-grained sediments as well as palynologic data combined with those from previous works (Belmonte 1966; Chevalier 1982; Njike Ngaha and Eno Belinga 1987; Ntamak-Nida et al. 2008; Njoh et al. 2013a,b, 2014, 2018; Njike Ngaha et al. 2014) to depict the depositional environment, the geodynamic context and the paleogeographic settings of the three sub-basins in order to establish a reliable correlation between these sub-basins and other basins in the West African margin, such as the coastal basins in Gabon (Teisserenc and Villemin 1989; Dupre et al. 2007; Chen et al. 2013), Nigeria (Adediran et al. 1991; Boboye and Okon 2014; Madukwe 2019; Oyebanjo et al. 2021), and those along the East Brazilian margin (De Ros et al. 2033; Valença et al. 2003) with share the same broad geological history.

We have also to note that the fine-grained sediments (very abundant in the Rio-del-Rey sub-basin) are more useful to constrain geochemical signature than the coarse ones (Taylor and McLennan 1985).

2. Geological Setting

The Cameroon Atlantic basin is structured from the south to the north by the Campo, Douala and Rio del Rey sub-basins. Each sub-basin comprises an offshore and an onshore part, and the present work concerns only the onshore outcrops.

The onshore part of the Campo sub-basin covers a surface of approximately 45 km^2 (Ntamak-Nida et al. 2008, 2010), with outcrops located along the beach of Campo town. The deposits belong to the lower part of the basal sandstones « Grès de base » lithofacies of the lower/middle Cretaceous of the Atlantic Basin of Cameroon (Dumort 1968; Njike Ngaha and Eno Belinga 1987; Njike Ngaha et al. 2014). The deposits, probably more than 500m thick, are characterized by a piedmont continental and lacustrine sedimentation in the open coastal zone on a narrow sea (Njike Ngaha and Eno Belinga 1987). The stratigraphic column (Fig. 2C) shows an alternation of conglomerates, arkosic sandstones, micaceous and ligneous claystones or shales and siltstones (Andreef 1947; Reyre 1959; Njike Ngaha and Eno Belinga 1987). These facies are frequently calcareous with varied concentrations. The sedimentary succession is characterized by a major retrogradation/progradation cycle with a well-developed progradation trend of the facies (Ntamak-Nida et al. 2010). At the basin margin, fluctuations in the lacustrine setting and sediment supply were controlled by active faults (Ntamak-Nida et al. 2010). The sedimentation took place in a series of asymmetrical horst- and-graben basins affected by a combination of N-S faults crossed by N60°E trending faults induced by the transformed movement of the South Atlantic (Benkhelil et al. 2002).

In the Douala sub-basin, covering about 6900 km^2 (onshore surface), seven formations are reported (Nguene et al. 1992), and some new terminologies have been proposed (Tchouatcha et al. 2021) since the former terminologies didn't completely match the specific scheme of the stratigraphic guide. These new proposed (informal ‘formations’) terminologies and the stratigraphy of the Cretaceous (Fig. 2B) of the Douala sub-basin are hereafter presented from bottom to top as follows:

- **The Mundeck Formation**: (?) Albian-Turonian, composed of continental to fluvio-deltaic deposits (fine-grained to conglomeratic sandstones with clayey silty intercalations) and rare interbedded shallow marine facies (Njike Ngaha and Eno Belinga 1987; Nguene et al. 1992);
- **(?) The Loungahé formation** (formerly Logbadjeck Formation): Coniacian-Campanian,), composed of fluvio-deltaic deposits lying in conformity or unconformity on the Mundeck Formation. The facies consist of micro-conglomerates, sands or weakly consolidated medium- to coarse-grained sandstones, silty and sandy clays, and limestones with marly calcareous intercalations (Njike Ngaha and Eno Belinga 1987);
- **(?) The Moungo formation**: Upper Campanian-Maastrichtian (formerly Logbaba Formation), only recognized through drilling and composed of weakly consolidated sands and sandstones, clays with

locally sandstones, schistose clays and limestones (Njike Ngaha, 1984), in conformity or unconformity on older formations.

In the Rio del Rey sub-basin, the stratigraphy exhibit seven units (Njoh et al. 2013), with four belonging to the Cretaceous (Fig. 2A). From bottom to top they are the following:

- Neocomian-Albian unit ("Grès de base", Dumort 1968) made up of fluvio-lacustrine mudstones, sandstones and conglomerates overlying the Precambrian basement ;
- Albian-Cenomanian unit (Njoh et al. 2013a) consisting of thin beds of limestones and calcareous shales interbedded within dark grey and black shales ;
- Turonian-Coniacian unit (Njoh et al. 2013b) made up of dark grey calcareous shales interbedded by marlstones, limestones and siltstones.
- Campanian-Maastrichtian unit (Kita Formation, Njoh et al. 2013b) made up mainly of calcareous shales.

3. Methods

Thirty thin sections of the representative Cretaceous fine-grained facies were prepared at the University of Assiut (Egypt) and Langfang Rock Detection Technology Services Ltd in Hebei (China). The petrographic study was carried out at the Laboratory of Petrology and Structural Geology at the University of Yaoundé 1, Cameroon.

The X-ray diffraction (XRD) patterns were obtained from the laboratory of "Argiles, Géochimie et Environements Sédimentaires)" at the University of Liège, Belgium and the XRD Unit at the Sohag University, Egypt. The analyses were carried out on the bulk material (non-oriented powder with grinded particles < 50 µm) of clays, shales, or silty claystones from the three studied sub-basins. The XRD patterns were recorded over the 2-70^{o}2θ angular range for the bulk material. The step sizes used in the analysis were 0.02^{o}2θ, and the time per step was 0.25s. Seventeen new samples were analyzed.

Whole-rock geochemical analyses of thirty samples, among which twenty new samples, of fine-grained facies (clay /claystones, shales, siltstones, and very fine-grained sands/sandstones respectively from Campo, Douala, and Rio-del Rey sub-basins), were carried out at The Bureau Veritas Commodities, Vancouver, Canada. Samples (homogenized powders) were mixed with $LiBO_2/Li_2B_4O_7$ flux. Crucibles were fused in a furnace at 1000^{o}C. The cooled bead was dissolved in ACS grade nitric acid. Trace elements (including rare earth elements = REE) were determined by inductively coupled plasma mass spectrometry (ICP-MS). Inductively coupled plasma-atomic emission spectrometry (ICP-AES) was used to obtain major element oxides. Loss on ignition (LOI) was determined by igniting a sample split and then measuring the weight loss. The assay uncertainties varied from 0.1–0.04% for major elements, 0.1 to 0.5% for trace elements, and 0.01 to 0.5 ppm for rare earth elements. Accuracy for REE is estimated at 5% for concentrations > 10 ppm and 10% when lower.

The palynological analyses of 16 samples, among which ten new samples, were carried out in the laboratory of palynology of the Geology Department (Assiut University, Egypt) following the method described in Mahmoud (2000), focusing only on the discrimination of continental and marine species.

4. Results

4.1. Lithology

In the Campo sub-basin, the fine-grained sediments alternate with coarse-grained sediments (sandstones and conglomerates), but the area is widely dominated by coarse-grained facies. The fine-grained sediments are compact and greyish to very black in color, millimetric to metric in thickness, affected by varied sedimentary structures such as lamination, bedding (Fig. 3A), and convolution. The tectonic structures such as listric faults (Fig. 3B) affected these deposits. Their microstructures are varied, fine-grained. and iso- to hetero-granular (Fig. 4A and B), laminated (Fig. 4A) with sometimes micro-boudinage. The mineralogy consists of abundant quartz and feldspar (30–60%), followed by muscovite, which sometimes reaches up to 20% of the bulk, and organic matter (3–45%). Four lithofacies of studied fine-grained sediments were identified in the fine-grained deposits from the Campo sub-basin; the massive or thin laminated claystones (Fml), the heterolothic mixture of claystones and siltstones interbedded with fine-grained sandstones (Fhl), the massive of thin laminated claystones/ siltstones with coal fragments (Fmlc) and the massive fine-grained sandstones (Sm) and described in Fig. 1a.

In the Douala sub-basin, the deposits are also widely dominated by coarse-grained facies. The fine-grained deposits show varied colors: dark (Fig. 3C), greenish (Fig. 3D), green yellowish (Fig. 3E), greyish, white greyish, reddish to mottled (Fig. 3F, G and H) and their thickness ranges from a few centimeters to metric. Contrarily to the Campo deposits, the Douala deposits are weakly consolidated. The microstructures are clastic and iso- to heterogranular (Fig. 4C, D, E and F) and sometimes laminated. Quartz is the most abundant mineral (40–50%), sometimes associated with feldspar (5–10%), muscovite (3–8%) and an undifferentiated matrix (20–35%). Four lithofacies are also identified in the fine-grained deposits from the Douala sub-basin; the massive claystones/siltstones (Fm), the massive or thin laminated claystones with abundant macrofossils (leafs or gastropods and bivalvia, Fmlf)), the horizontal and laminated claystones/siltstontes (Fhl) and the very fine-grained sandstones (Sm) and described in Fig. 1b.

In the Rio-del-Rey sub-basin, the facies are mainly fine-grained with carbonate minerals (siderite, dolomite, and calcite). Their colors are greyish, greenish grey and dark (Fig. 3I and J). The thickness ranges from decametric to plurimetric. The main sedimentary structures are bedding and lamination (Fig. 3I). The microstructures are cryptocrystalline, clastic and iso- to sub-isogranular (Fig. 4G, H, I and J). The dominant mineral is quartz, with rare siderite. The organic matter concentration ranges from 3 to 35%. Four lithofacies were also identified in the fine-grained deposits from Rio-del-Rey sub-basin; The massive claystones (Fm), the massive or thin laminated claystones (Fml), the horizontal and and laminated marlstones/ calcareous claystones (Fhl) and the massive of thin laminated claystones with bivalvia (Fmlf) and described in the Fig. 1c.

4.2. Geochemistry

- **Major elements**

Table 1 displays the major elements composition of the thirty studied samples from the sub-basins. SiO_2 (10.23–88.89%), Al_2O_3 (4.2-24.95%) and Fe_2O_3 (0.25–39.89%) are the dominant phases. The Douala facies show the highest SiO_2 content (46.47–88.89%), followed by the Campo (43.48–61.75%) and lastly by the Rio-del-Rey (10.23–56.19%) facies. The lowest and highest Al_2O_3 concentrations (4.2% and 24.95%) are found in the Douala sub-basin. The highest Fe_2O_3 concentrations are observed in the Rio-del-Rey deposits (7.01%-39.89%), followed by those of the Campo (4.2–8.42%) and lastly by those of the Douala (0.25%-7.97%) deposits.

Table 1: Lithofacies of Cretaceous outcrops from Atlantic Basin of Cameroon. The facies codes are from Miall (1996), and Ntamak-Nida et al. (2010). The interpretations provided are according to Lowe (1982), Miall (1996) and polynologic data

Table 1
a: Cretaceous outcrops from Campo sub-basin

Facies code	Facies name	Lithology	Structure	Depositional processes and environment
Fml	Massive or thin-laminated claystones /siltstones	Claystones and siltstones, well to poorly sorted, greyish to dark, micaceous (muscovite essentially), angular to very angular grain shapes	Massive or thin laminated, schistosity, mica with sigmoid shape, 5 to 180 cm thick, sharp boundary	Deposition from suspension (Miall, 1996) or rapid deposition due to ponding of fine-grained turbidity current. Lacustrine environment
Fmlc	Massive or thin-laminated claystones /siltstones with coals	Same like Fml with centimeter to decimeter-size of coal fragments, poorly sorted	Same like Fml	Same like Fml
Fhl	Heterolitic claystones / siltstones	Mixture of claystones and siltstones or very fine sandstones	Laminated or bedding, 5 to 100 cm thick, sharp boundary	Low energy flow, deposition from suspension (Miall, 1996), rapid variation of sedimentation conditions. Fluvio-lacustrine environment
Sm	Massive sandstones	Fine-grained sandstones, moderately to poorly sorted, greyish, sub-angular to angular grain shapes with some sub-rounded shapes	Massive, monoclinal, 5 to 100 cm thick, sharp boundary	Rapid deposition of fine-grained sands from turbulent suspension (Lowe, 1982). Fluvio-lacustrine environment

Table 1

b: Cretaceous outcrops Douala sub-basin

Facies code	Facies name	Lithology	Structure	Depositional processes and environment
Fmlf	Massive or thin-laminated claystones with fossils	Fine grained- to sandy claystones, well to poorly sorted, greyish dark, abundant leafs or bivalvia fossils and microfossils (Dinoflagellates, pollens spores, Foraminifera lining)	Massive or thin laminated or fissils, 100 to more than 200 cm thick, erosive boundaries	Deposition from suspension (Miall, 1996) or rapid deposition due to ponding of fine-grained turbidity current. Shallow marine environment
Fm	Massive claystones	Claystones to silty claystones, moderately to well sorted, reddish, greenish, grey whitish or mottled, angular grain shapes	Massive, 10 to up than 200 cm thick, erosive boundaries witth sandstones	Lower energy flow, deposition from suspension (Miall, 1996) or rapid deposition due to ponding of fine-grained turbidity current. Fluvio-deltaic environment
FL	Laminated claystones	Same as Fm, but frequently mottled	Laminated, 10 to 30 cm thick, erosive boundaries	Same to Fm, with rapid variation of sedimentation environment, Fluvio-deltaic environment
Sm	Massive sandstones	Fine-grained sandstones, moderately to poorly sorted, angular to very angular grain shapes, reddish to grey whitish	Massive, 50 to 150 cm thick, erosive boundaries with claystones	Rapid deposition of fine-grained sands from turbulent suspension (Lowe, 1982). Fluvio-deltaic environment

Table 1

c: Cretaceous outcrops from Rio-del-Rey sub-basin

Facies code	Facies name	Lithology	Structure	Depositional processes and environment
Fml	Massive or thin-laminated claystones /marlstones	Fine grained-claystones/marlstones, well to moderately sorted, greyish dark to greenish grey, microfossils (Dinoflagellates, pollens, spores, Foraminifera)	Sharp boundary slightly to highly fissile, 100 to > 300cm thick	Low energy flow, deposition from suspension or from weak traction current (Miall, 1996). Marginal to shallow marine environment
Fl	Lamimated calcareous /carbonated shales/siltstones	Fine-grained calcareous/ carbonated shales/ siltstones, well to moderately sorted, whitish to greenish grey color, microfossils (Dinoflagellates, pollens, spores)	Sharp boundary, 1 to 20cm thick, lamination	Deposition from suspension (Miall, 1996). Marginal marine environment
Fmlf	Massive or thin-laminated claystones / marlstones with fossils	Same to Fml with more or less abundant and varied bivalve fossils (moulds essentially), microfossils	Sharp boundary slightly to highly fissile, 100 to 400 cm or > 400 cm thick	Same to Fml
Fm	Massive claystones	Fine-grained calcareous/ carbonated claystones, well sorted, dark grey, microfossils	Lenticular or nodular beds, sharp boundary, 2 to 7 cm thick	Rapid deposition from weak traction current (Miall, 1996). Shallow marine environment

The second most abundant group of oxides includes MgO (0.06–7.95%), CaO (0.01–10.49%), K_2O (0.09–6.48%), Na_2O (0.01–2.37%). By comparison, the Douala deposits are the least enriched in MgO (0.06–2.39%) while the Kribi-Campo and Rio-del-Rey deposits show the highest MgO concentration, respectively (1.93–6.15%) and (0.89–6.95%). CaO concentrations are very low in the Douala deposits (0.01–0.09%) and higher in the Rio-del-Rey (0.04–16.26%) and Campo (0.52–6.91%) deposits. K_2O concentrations are relatively low in the three sub-basins, however, with some differences in the Rio-del-Rey deposits where K_2O varies from 0.37–3.48%. The K_2O content is higher in the Campo (2.68–4.76%) and Douala deposits (0.1–6.48%). NaO_2 concentrations are lower in the Douala deposits (0.01–0.09%) than in the Rio-del-Rey (0.04%-2.37%) and in the Campo (0.93–1.74%) deposits.

The least abundant group of oxides includes TiO_2, P_2O_5, MnO, and Cr_2O_3. TiO_2 concentrations vary between 0.15% and 1.93%, 0.24% and 1.31% and 0.49% and 1.17% respectively for the Rio-del-Rey, Douala, and Campo sub-basins. P_2O_5 concentrations are ≤ 0.35%, but lower (0.01%- 0.15%) in the Douala deposits. MnO concentrations are generally ≤ 0.22% and only one sample shows concentrations 1% (1.04%) in the Rio-de-Rey sub-basin. Cr_2O_3 is the least concentrated element, with concentrations 0.02%.

The analysis of the spider plot of average major elements normalized to PAAS (Fig. 5A) shows that SiO_2, Al_2O_3, Na_2O, K_2O, and TiO_2 are depleted in the three sub-basins, with the highest depletion of Na_2O in the Douala sub-basin. However, CaO and Fe_2O_3 show high concentrations in the three sub-basins, with the highest CaO content (16.26%) in the Rio-del-Rey sub-basin. Unlike the deposits from the Rio del Rey and Campo sub-basins which are slightly carbonated, those from the Douala sub-basin are mostly terrigenous in the lower part of the sequence. The carbonate facies (Isue et al., 2021) are mainly present at the top of the Douala sequence (Njike Ngaha et al. 2014).

Figure 6 shows that the fine-grained Cretaceous facies consist mainly of shales and Fe-shales in the three sub-basins, those from the Campo sub-basin corresponding exclusively to shales. The Douala facies are more diversified with Fe-sands, arkoses and sub-arkoses.

- **Trace elements**

Table 2 displays the trace element distribution in the studied samples from the sub-basins. The most abundant include Ba (70 -1548 ppm), Zr (91–524 ppm) and Sr (7.2-388.9 ppm). Ba is averagely and constantly present in the Campo deposits (502–768 ppm). However, its concentration fluctuates and ranges from 70 to 518 ppm in the Rio-de-Rey deposits and from 95 to 1548 ppm in the Douala deposits. Zr content fluctuates and ranges from 91.7 to 638.6 ppm, from 144.3 to 668.3 ppm and from 131.3 to 337.9 ppm, respectively in the Rio-del-Rey, Douala and Campo sub-basins. It is worth noting that the Campo has the lowest Zr concentration. Sr concentrations also depict fluctuations in the three sub-basins (see Table 2).

However, the spider plot of average trace elements normalized to PAAS (Fig. 5B), depicts a depletion of Ba in the three sub-basins, while Sr is depleted in the Campo and Douala sub-basins and slightly concentrated in the Rio-del-Rey sub-basin. Zr shows elevated concentrations in the three sub-basins. Other elements such as Ni and Rb are depleted in the three sub-basins, while U is depleted in the Douala and enriched in the Rio-del-Rey and Campo sub-basins. Hf and Y show high concentrations in the three sub-basins.

- **Rare Earth Elements (REE)**

Table 3 shows that the ΣREE concentrations in the studied sediments range from 154.64 to 339.08 ppm, from 60.57 to 725.16 ppm and from 107.63 to 265.56 ppm, respectively for the Rio-del-Rey, Douala and Campo sub-basins. The LREE contents are higher as compared to the HREE in the three sub-basins and their ratios (LREE/HREE) range from 9.41 to 21.70, from 11.25 to 24.89 and from 9.05 to 14.50

respectively, for Rio-del-Rey, Douala and Campo sub-basins indicating enrichment in LREEs in the three sub-basins (Table 3).

The REE patterns (Fig. 7A) normalized to PAAS (McLennan, 2001) are quite flat with positive Eu anomalies. The more depleted and enriched sediments are from the Douala sub-basin.

The REE patterns (Fig. 7B) normalized to chondrites (McDonough and Sun 1995) are quite similar with LREE enrichment compared to HREE.

The LREE/HREE ratios range from 9.41 to 21.70, from 11.25 to 24.89 and from 9.05 to 14.50 suggesting low to moderate (Rio-del-Rey sub-basin), moderate to high (Douala sub-basin), and low to moderate (Campo sub-basin) fractionation of REE.

The studied samples show no to slight positive Eu anomalies (Eu/Eu*: 1.02–1.32) and slight negative to no Ce anomalies (Ce/Ce*: 0.85–0.97) in the Rio-del-Rey sub-basin; negative to positive Eu anomalies (Eu/Eu*: 0.61–1.46) and negative to no Ce anomalies (Ce/Ce*: 0.66–1.04) in the Douala sub-basin; and no to positive Eu anomalies (Eu/Eu*: 0.98–1.28) and no Ce anomalies (Ce/Ce*: 0.93–0.95) in the Campo sub-basin.

The Ce/Ce* Vs Pr/Pr* plot of Bau et al. 1996 (Fig. 7C) was used to discriminate the “real” from “false” Ce anomaly in the sediment due to the possible anomalous abundance of La. Most of the samples from Douala sub-basin plot into field IIIb (negative Ce anomaly). The samples from Rio-del-Rey and Campo sub-basins associated with some from Douala sub-basin are grouped at the limit between field IIa (positive La anomaly, no Ce anomaly) and field I (neither Ce nor La anomaly).

4.3. X-Ray diffraction

In the southern part of the Douala sub-basin, two groups of minerals have been found, i.e. clays and non-clays. Clays consist of kaolinite, vermiculite, illite in various amounts, and non-clays consist of large amounts of quartz, magnetite, and goethite, and small amounts of feldspar (Fig. 8a). Kaolinite is found in the northern part of the Doula sub-basin; where mineralogy is dominated by quartz and feldspar, with magnetite and goethite being the least abundant minerals (Fig. 8b).

In the Rio-del-Rey sub-basin, there are two groups of materials with different ages: the lowest part of the sequence has an Albian-Cenomanian age and its upper part a Campanian-Maastrichtian age.

The Albian-Cenomanian mineralogy is made up of the aforementioned minerals. Clays are dominated by kaolinite, chlorite, and illite. It is worth noting that the amount of clay minerals in the Albian-Cenomanian gradually decreases from bottom to top.

Non-clays are represented by the dominant quartz, feldspar, and magnetic minerals associated with dolomite and calcite, whose amount generally decreases from bottom to top. In the Campanian-Maastrichtian series, the clays are mainly made up of kaolinite increasing from bottom to top, depicting a different trend with respect to the Albian-Cenomanian part. The non-clays are dominantly made up of quartz, feldspar, and magnetite, which may be associated with dolomite and siderite. The siderite is sometimes more concentrated than the quartz (Fig. 8c).

In the Campo sub-basin, the amount of clays is low and kaolinite appears to be the only dominant phase. However, it should be noted that kaolinite is less abundant in claystones rich in organic matter. Non-clays are composed of quartz (more abundant), feldspar, muscovite, dolomite, magnetite, goethite, and a slight amount of calcite and biotite (Fig. 8d). Muscovite and dolomite are less abundant in the claystones.

4.4. Palynological data

- **Campo sub-basin**

Analysis of five samples (TCA1, TCA2, TCA3, TCA4 and TCA5) collected along the stratigraphic column shows generally a poor diversified palynological content with only abundant phytoclasts/organic matter. The palynological species (samples TCA2 and TCA3) consist exclusively of continental forms, largely dominated by xerophytic pollens such as *Classopollis* sp. (Fig. 9N), associated with *Eucommiidites troedssonii* (Fig. 9M), *Ephedripites* sp. and *Deltoidospora* sp. (Fig. 9O) and spores such as *Cicatricosisporites* sp.

- **Douala sub-basin**

Among the eight studied samples, six were barren (greenish, reddish, and mottled samples). Only two samples (TDBAN and TDMAN) were productive, the black clays belonging to the Moungo Formation (Cenomanian to Turonian) and located respectively in the localities of Mbanga and Ediki, about 3 to 5km apart. The Mbanga and Ediki formations, which may be correlated, are composed of a diverse sporopollenic association with known continental and marine species (Njike Ngaha et al. 2014; Njoh et al. 2014) however, with some differences.

At Ediki (sample TDMAN), the palynological content shows a more or less abundance of xerophytic species such as *Classopollis* sp. and *Ephedripites* sp. associated with other pollens such as *Triporopollenites* sp., *Tricolpites* sp. (Fig. 9F), *Araucariacites* sp, *Stellatopollis* sp., *Inaperturopellenites* sp, and others, spores of Pteridophytes such as *Todisporites* sp., spores of fungi such as *Pluricellaesporites* sp., *Dicellaesporites* sp., unicellular form (Fig. 9R) and marine palynomorphs such as microforaminiferal ligning (Fig. 9K, and 9S). Njoh et al. (2014) also reported in the same area rare dinoflagellates. The continental species concentration ranges between 95 to 97% and the marine ones 3 to 5% (Fig. 11).

At Mbanga (sample TDBAN), clays are very rich in phytoclasts (leafs) and the sporopollenics are dominated by xerophytes *Classopollis* sp., and *Ephedripites* sp. (Fig. 9G) with *Crybelosporites panuceus* (Fig. 9H) and others, the spores of which are Pterophytes, fungi, and marine species (foraminiferal test lining) (Fig. 9Q and 9U). The continental species concentration ranges between 93 and 95% and the marine ones 5 to 7% (Fig. 11).

- **Rio-del-Rey sub-basin**

Two samples (MK2 and DK1B) were analyzed for the palynological content respectively at Mesambi downstream (Albian-Cenomanian) and Djega localities (Campanian-Maastrichtian) as reported in Tchouatcha et al. (2022). The palynological content of MK2 is very rich in non-marine species (96–98%) (Fig. 11) with an abundance of xerophytes such as *Ephedripites* sp. (Fig. 9A) and *Classopollis* sp., associated with *Elateroplicites africaensis* (Fig. 9B), *Spheripollenites* sp. (Fig. 9C), *Cretacaeiporites mulleri*, *Araucariasites* sp. (Fig. 9V) and other (Pteridophyte spores, Fungi,). Marine species (2–4%) (Fig. 11) are represented by rare microforaminiferal lining and dinoflagellates such as *Dinopterygium cladoides*. Meanwhile, the palynological data from this outcrop indicate a marine species abundance between 0 and 4.2% (Njoh et al. 2013). The palynological content of DK1B is also rich in continental species (86–88%) (Fig. 10) such as *Echitriporites trianguliformis* (Fig. 9E), *Monocolpate* sp. (Fig. 9I), *Spinozocolpites baculatus* (Fig. 9J) associated with marine species (12–14%) (Fig. 11), foraminifera and especially dinoflagellates (*Cerodinium* sp., Fig. 9T) reported here for the first time. Note that the studied outcrop has revealed a diversified planktic and benthic foraminiferal content (Njoh et al. 2018).

5. Discussion

- **Provenance**

Roser and Korsh (1988) have proposed a diagram allowing recognition of lithologies, including felsic, intermediate, mafic, and recycled-mature quartzose provenance (Fig. 10A). The studied sediments are plotted in recycled quartzose (2 samples), intermediate igneous (3 samples) and mafic igneous (4 samples) provenance fields for the Rio-del-Rey deposits, in recycled quartzose (10 samples), felsic igneous (2 samples) and mafic igneous provenance fields (3 samples) for the Douala deposits, and in recycled mature field for all samples from the Campo deposits. The plotted sediments in the recycled field may indicate the para-derived metamorphic source rocks with preserved sedimentary signatures and /or more not well-known ancient deposits.

Other plots such as Ce vs. La/ Nb (Rao et al. 2011) (Fig. 10B) and La/Th vs. Hf (Floyd and Leveridge, 1987) (Fig. 10C) have also been widely used (e.g. Moradi et al. 2016; Zeng et al. 2019; Tchouatcha et al. 2021) for Ce vs. La/Nb and Ngueutchoua et al. (2019a, b) and for La/Th vs. Hf). The Ce vs. La/ Nb scattered plot applied to our study points to a dominant felsic source with a contribution of an intermediate igneous source for the Rio-del-Rey and Douala deposits, contrary to the Campo deposits showing a dominant intermediate igneous source with a felsic contribution. The La/Th vs. Hf plot shows that the Campo deposits derived mainly from felsic rock sources, the Rio-del-Rey deposits from felsic and mixed felsic and intermediate composition source rocks, and the Douala deposits from mainly felsic composition in the northern part, and mixed felsic and intermediate to intermediate composition in the southern part.

Some elemental ratios are useful in unravelling the source signatures of sediments, such as Th/Co (Cullers 2000; Armstrong et al. 2015) and Al_2O_3/TiO_2 (Absar and Sreenivas 2015; Zhou et al. 2015; Tchouatcha et al. 2021b). The Th/Co ratio value ranges from 0.67–19.4 and 0.04 to 1.10 respectively, in felsic and mafic sources. For the sediments studied here, the ratio varies from 0.39 to 1.82, with main values 1 in the Rio-del-Rey deposits, from 0.62 to 13.75 in the Douala deposits with high values in the northern part of the sub-basin (0.62–13.75; average: 4.56) and low values in the southern part (0.69–1.35; average: 1.07); and from 0.51 to 0.98 in the Campo deposits, indicating respectively a felsic source with contribution of mafic source in the Rio-del-Rey sub-basin, a dominant felsic source in the northern part of the Douala sub-basin and dominant intermediate source in the southern part, and the intermediate source in the Campo sub-basin. The Al_2O_3/TiO_2 ratio varies from 3 to 8, 8 to 21 and 21–70 respectively for mafic, intermediate and felsic igneous sources (Hahashi et al. 1997). In this study, the ratio ranges from 10.12 to112.93 (average: 26.29) in the Rio-del-Rey deposits, 8.57 to 30.37 in the Douala deposits, with more high values in the northern part (16.45 to 30.37, average: 21.06) and low values in the southern part (8.57 to 21.90, average: 15.68), and 14.04–21.78 (average: 16.37) in the Campo deposits. This also indicate respectively felsic rocks with contribution of mafic rock in the Rio-del-Rey deposits and dominant felsic rocks in the northern part of the Douala deposit and intermediate rock composition in the southern part, and intermediate rock composition in the Campo deposits.

Furthermore, the REEs and relevant parameters are also useful to characterize the lithotype rock source of sediments (e.g. Liu et al. 2015; Ma et al. 2015; Zeng et al. 2019; Tchouatcha et al. 2021), and the higher LREE/HREE ratio and low Eu anomaly indicate a felsic igneous source, whereas the lower LREE/HREE ratio and relative high Eu anomaly reflect a mafic igneous source (Armstrong-Altrin et al. 2013). The LREE/HREE ratios range from 9.05 to 14.50 and no to slight positive Eu anomaly (0.98 to 1.28) in the Campo deposits, 15.34 to 24.03 and negative to positive Eu anomaly (0.61 to 1.46) in the southern part of the Douala sub-basin, 11.25 to 24.89 and no to slight positive Eu anomaly (1.03 to 1.35) in the northern part of the Douala sub-basin, and 9.41 to 21.70 and no to slight positive Eu anomaly (1.04 to 1.32) in the Rio-del-Rey deposits, indicating respectively intermediate composition for Campo deposits, predominance of felsic composition in the northern part of the Douala sub-basin with no to slight positive Eu anomaly, predominance of intermediate of mixed of felsic and mafic composition in the southern part of the Douala sub-basin with negative to positive Eu anomaly, and predominance of felsic composition of the source rocks in the Rio-del-Rey sub-basin. The Fig. 11 shows the varied source rocks lithology of the three sub-basins along the Atlantic Ocean.

Figure 12 shows that samples from the Douala sub-basin plot close to and along the A-K apex suggesting either the lack of plagioclase and occurrence of K-feldspar (orthoclase) in the source rocks or diagenetic effects by post-depositional conversion of clays such as kaolinite to illite by including K^+ in their structure (Fedo et al. 1995). As the diagenetic effects are very weak (early diagenesis, see part 5.5), the samples plot close A-K apex indicate a high degree of weathering of the source rocks containing abundant K-bearing minerals. Similar results were given in detrital Cretaceous outcrops in the northern part of this sub-basin (Ngueutchoua et al. 2017, 2019; Esue et al. 2021). Meanwhile, some samples, precisely limestones and marly limestones, show a low to very low degree of alteration probably due to chemical input or origin of these deposits (Esue et al. 2021). Figure 12 also indicates a low to high weathering of the Rio-del-Rey sub-basin deposits and moderate weathering of the Campo sub-basin deposits. It also shows that the varied source rocks for each and all the three sub-basins experienced varied weathering degrees. Moreover, the presence of volcanic fragments (basaltic pebbles), reported in the Upper Cretaceous sandstones of Santos Basin, Eastern Brazilian Margin (De Ros et al. 2003), in the Cenomanian-Turonian deposits (Njike Ngaha 1984) in the north of the Douala sub-basin highlighst a volcanic activity which took place probably during the Albian rifting reported as well as in the Sergipe-Alagoas Basin (North-eastern Brazilian Coastal Basin) and the North Gabon (Western African Coastal Basin) (Kurobaza et al. 2018).

5.2. Sediment sorting, maturity, recycling and paleoweathering

The ICV (Index of Compositional Variability; Cox et al. 1995) and CIA (Chemical Index of Alteration; Nesbitt and Young 1982) (Fig. 13) are widely used to characterize the compositional maturity of sedimentary deposits (e.g. Mongelli et al. 2006; Perni et al. 2011; Tao et al. 2013, Armstrong-Altrin et al. 2015; Tawfik et al. 2017; Tchouatcha et al. 2021b). Figure 13 shows that sediments from the Campo sub-basin are globally sub-mature (ICV: 0.98 to 2.12, average: 1.48; CIA: 65.26 to 74.72; average: 70.24). The sediments from the Douala sub-basin are mature (ICV: 0.37 to 0.90) with intense chemical weathering of the source area (CIA: 67.00 to 99.33), whereas the sediments from the Rio-del-Rey sub-basin are sub-mature to mature with two samples (MK3 and DK1A) showing high ICV values (5.04 and 10.03) and high CIA (77.38 and 92.04) respectively.

The PIA (Plagioclase Index of Alteration; Nesbitt and Young, 1982; Fedo et al. 1995) is also used to characterize the chemical weathering of source rocks (e.g. Rashid et al. 2015, Ngueutchoua et al. 2019a, Tchouatcha et al. 2021b). The high values (PIA 75) and low values (PIA $\leq$ 50) of PIA reflect respectively intense and weak chemical weathering of these rocks. Table 1 shows that in the Campo sub-basin, the PIA of the sediments ranges from 72.70 to 87.57 reflecting moderate to high chemical weathering, from 96.35 to 99.90 in the Douala sub-basin indicating high chemical weathering, and 66.68 to 99.47 in the Rio-del-Rey sub-basin suggesting weak to high chemical weathering.

Meanwhile, due to the high carbonate proportions in the main samples from Campo and Rio-del-Rey sub-basins compare to those from Douala sub-basin, the PIX and CIX, without CaO (Garzanti et al. 2014; Garzanti et al. 2019) were used to better correlate and appreciate the weathering degree of samples from the three sub-basins. Table 1 shows that CIX and PIX range respectively from 71.26 to 76.88 and from 84.19 to 92.25 in the Campo sub-basin indicating moderate to high chemical weathering, from 67.15 to 99.39 and from 96.94 to 99.94 in the Douala sub-basin suggesting weak to high chemical weathering, and from 73.77 to 92.90 and 80.15 to 99.64 in the Rio-del-Rey sub-basin indicating moderate to high chemical weathering.

5.3. Paleoclimate and the depositional environment

The CIA and PIA indices and some trace element ratios such as Rb/Sr are reliable tools for paleoenvironment characterization (e.g. Cao et al. 2012, Hernandez-Hinojosa et al. 2018, Ekoa et al. 2021, Tchouatcha et al. 2021b). The clay minerals record the condition and climatic fluctuation of the sedimentary environment (Singer 1988, Meng et al. 2012). It is worth noting that at each stage of transformation, clay minerals respond to their chemical and thermal environment, and, as a consequence, their properties and species change. Kaolinite is formed in a subtropical humid climate by the intense weathering of feldspar. Illite is mainly formed in a cold climate with low precipitation. Chlorite and illite form the basis of the diagenetic zone (Dunoyer De Segonzac 1970). Al_2O_3 vs. V and Al_2O_3 vs. P_2O_5 are also useful for paleoenvironmental conditions and have been successful used (e.g. Mortazavi et al. 2014; Anaya-Gregorio et al. 2018; Ekoa et al. 2021). Variation of phosphorus concentration is controlled by water depth and temperature and vanadium concentration is somewhat higher in marine facies than in freshwater sediments. The diagrams Al_2O_3 vs. V (Fig. 14A) and Al_2O_3 vs. P_2O_5 (Fig. 14B), show that sediments from the three sub-basins were deposited in shallow marine and fluvial environments at various depths suggested by relatively low and varied concentrations of vanadium. The plotted sediments from Campo and Rio-del-Rey sub-basins generally indicate important depth, those from Douala sub-basin, on the contrary, formed in a low water depth with poorer phosphorus concentrations.

The Sr/ Ba ratio has been widely used for salinity conditions (e.g. Zheng and Liu 1999; Meng et al. 2012; Zeng et al. 2019; Tchouatcha et al. 2021b). These ratios increase from coastal fresh water to the open and saline marine water (Cao et al. 2012), and are > 1 in marine and 1 in freshwater sediments (Jones and Manning 199; Shi et al. 1994; Wang et al. 2005). In our study, sediments from Rio-del-Rey have higher values (0.41 to 1.07) while those from the Douala (0.09 to 0.85) and Campo (0.20 to 0.31) sub-basins are low, indicating a dominant marine influence in the Rio-del-Rey sub-basin and predominant continental conditions in the Douala and Campo sub-basins.

The high CIA values indicate warm and humid climatic conditions during sediment deposition (Nesbitt and Young 1982). In the Rio-del-Rey sub-basin, CIA values range from 63.59 to 92.76 suggesting less humid climatic variation in the Albian-Cenomanian, while in the Campanian-Maastrichtian, CIA values vary between 92.04 and 92.76), suggesting more humid climatic conditions. In the Douala sub-basin, this ratio varies from 67.00 to 99.33, and is particularly high (92.11 to 99.33) in the southern part and low (67.00-83.58) in the northern part, highlighting the influence of the source rock lithology, felsic in the northern part and intermediate to mafic in the southern part. In the Campo sub-basin, this ratio ranges from 65.26 to 74.72 indicating semi-arid conditions.

The SiO_2 vs. $Al_2O_3 + Na_2O + K_2O$ plot (Fig. 14C) shows that the Campo and Rio-del-Rey sediments have been deposited under semi-arid to arid conditions, while those from Douala may have been deposited under semi-arid to arid with periodically semi-humid conditions (fine-grained sands), probably linked to the marine influence.

In the Campo sub-basin, the palynological species consist exclusively of continental forms. Previous palynological data (Belmonte 1966; Chevalier 1982; Ntamak-Nida et al. 2008) did not support the presence of marine species in these deposits. In addition, Andreef (1947) reported some ammonite specimens, leading to the conclusion that the deposits in the Kribi-Campo sub-basin were related to piedmont continental and lacustrine settings near a coastal zone open to a narrow sea (Njike Ngaha et Eno Belinga 1987). More, the presence of dolomite may indicate either elevated temperature and pressure conditions during diagenesis or is related to the circulation of restricted marine pore waters near the mixing zone, as it is the case in the Mamfe Basin (Eyong 2003). In the case of Campo sub-basin, the second hypothesis seems plausible in the context of the rifting of this sub-basin and the presence of dolomite in one part (upper part, See Fig. 8d) of deposits. The presence of the *Botryococcus* sp. (freshwater algae, Ntamak-Nida et al. 2008,) in these deposits could confirm the continental environment with periodical marine influence.

The abundance of phytoclasts (leafs) at Mbanga in the Douala sub-basin may indicate that these deposits are more continental, as suggested by their proximity with the margin outcrops such as the conglomeratic sandstones. The marine species in these deposits indicates a marine influence during the Cenomanian (Njike Ngaha and Eno Belinga 1987; Njike Ngaha et al. 2014; Njoh et al. 2014), with a shallow environment at Ediki and a marginal to shallow marine setting at Mbanga. At Ediki, the black clays are intercalated between the sandstone facies, while at Mbanga, they are exposed and found on top of the poorly consolidated sandstones, reflecting intense erosion towards the basin margin or differential erosion. Furthermore, two sediment cycles during the Cretaceous have been recognized in the Douala sub-basin from drilling and seismic surveys on land, in swamps, and sea (Seiglie et al. in Regnoult 1986), one cycle of low amplitude between the Cenomanian and the Turonian, and the other of high amplitude between the Coniacian and the Maastrichtian.

The marine species in the Cenomanian and Campanian-Maastrichtian of the Rio-del-Rey sub-basin reveal a marine influence. The more abundant and varied marine species in the Campanian-Maastrichtian point to a more offshore environment as compared to that of the Cenomanian. This is also reported by Njoh et al. (2016, 2018).

On the southern part of the Douala sub-basin, the low proportion or even absence of kaolinite on the one hand, and on the other hand, the feldspar whose alteration produced kaolinite, suggest that the source rock was poor in feldspars and richer in ferromagnesian minerals as also suggested by the geochemical data. The hypothesis of a subtropical climate (warm and relatively humid) can be considered by chlorite/vermiculite, iron oxides and hydroxides such as magnetite and goethite. In the northern part, the low abundance of kaolinite associated with magnetite suggests hot and semi-arid climatic conditions during the Albian-Cenomanian to Turonian times.

In the Campo sub-basin, muscovite records a continental influence. The fluctuation of dolomite concentration suggests variation of the sedimentation, probably related to a marine influence. The fluctuation and low abundance of kaolinite point to semi-arid to arid climatic conditions.

In the Rio-del-Rey sub-basin, the mineralogical (kaolinite mainly) variation may indicate a climatic change from semi-arid to more arid conditions during the Albian-Cenomanian. The increase of kaolinite in the upper part indicates a climatic change from more arid conditions to semi-arid during the Campanian-Maastrichtian.

5.4. Behavior of chemical composition versus Al/ Si

To depict the grain size effect on geochemical composition of the sediments, Bouchez et al. (2011), Roddaz et al. (2014) and Tchouatcha et al. (2022) have used the Al/ Si ratio which is considered as a proxy for sediment grain size applied in the Amazonian floodplain sediments (Bouchez et al. 2011). Figure 15 shows the variation of Al/Si ratios vs. CIA and some element concentrations such as Na, Hf, Ca, K and Zr. According to this figure, Al/ Si shows no correlation with CIA, Hf and Zr for sediments from the three sub-basins, no correlation with Na and Ca for the Douala sub-basin sediments, negative correlation fort the Campo and Rio-del-Rey sub-basins sediments, no correlation with K for Douala and Rio-del-Rey sub-basins sediments and a positive correlation for the Campo sub-basin sediments. These varied behaviours and the pattern of enrichment and depletion of major and trace elements (Fig. 5A and B) could indicate the varied provenances of the material in the different environments of sedimentation of the three sub-basins.This is also confirmed the palynological data; fluvio-lacustrine environment for the Campo sub-basin, fluvio-deltaic with marine influence environment in the upper part for the Douala sub-basin and marginal to shallow marine environment for Rio-del-Rey sub-basin.

5.5. Diagenetic effects

- **Campo sub-basin**

The diagenetic signatures in the Campo sub-basin were depicted using X-ray diffraction (Fig. 8) and petrography (Fig. 4). X-ray diffraction data exhibit non-clays minerals such as quartz (abundant), feldspar, muscovite and a few biotite, clay minerals represented by kaolinite and chemical minerals made up of calcite and sometimes dolomite. Kaolinite can be diagenetic or detrital origin. In the case of diagenetic origin, kaolinite is the product of dissolution of potassic feldspars. The detrital one is linked to climatic conditions, from hydrolysis of alkaline feldspars, its presence in the sediments is indicative of rigorous weathering of source rocks with steep relief and exhaustive leaching of weathered materials under a warm, humid and acidic milieu (Enu, 1986).. The detrital origin for this study is expected because of permanent association of kaolinite with high quantity of quartz which is resistant to alteration and concentrates in sediments transported and deposited by rivers. In this case, kaolinite appears in low quantity (Fig. 8C), its low quantity and fluctuation, generally lower in the organic matter-rich levels (TCA2 and TCA3) could indicate the link with climate.

The carbonate minerals such as calcite and dolomite, could be authigenic or diagenetic. The authigenic mineral can precipitate directly from solution or from weathering and replacement during burial. Diagenesis is a set of physical and chemical processes which affect sediments after deposition until the limit with metamorphism (Blatt et al. 1972). Generally, the evidence of chemical diagenesis can be inferred from physical aspect. In this case, calcite fluctuates, being very low in the lower part of the studied series and low in the upper part. Its presence in the clayey matrix could be explained by precipitation from dissolution of unstable minerals (Tawfik et al. 2017) such as feldspars which are frequently vesicular and sericitized. In the sandy facies, calcite fills most of the secondary pores and is as mineral replacement (Ashukem et al. 2022). Dolomite fluctuates also, very low to absent in lower part of the studied series and high (the highest after quartz) in the upper part. This mineral can be diagenetic linked to temperature and pressure increase or results from the circulation of restricted marine pore water near a mixing zone (Eyong 2003). Its fluctuation supports the second hypothesis.

In thin section, phyllosilicates such as muscovite/ sericite, the most abundant mineral after quartz, show some packing readjustment with preferential orientation and sigmoid shapes (Fig. 4A), indicating a significant physical effect, as evidenced by varied type of inter-granular contacts such as plan, convexo-concave or sutured contacts in the sandy facies. Elsewhere, silica from dissolution of quartz, feldspar infillings in the pore spaces, and quartz and feldspar overgrowths are common in the sandy facies (Ashukem et al. 2022).

- **Douala sub-basin**

Contrary to the Campo and Rio-del-Rey sub-basins, the Cretaceous fine-grained deposits from the Douala sub-basin are poorly consolidated or friable indicating a low burial and weak compaction of these deposits. In the coarsest grained facies (poor consolidated siltstones or sandstones), the clay matrix occupies the large inter-granular pore spaces in the loosely packed detrital grains (rare contact points between quartz and feldspar) with a floating grain texture (Fig. 4F). X-ray diffraction did not reveal any carbonate minerals. Clays minerals such as kaolinite is very low or absent in the southern part of the sub-basin and present in its northern part, conversely for the chlorite or vermiculite, indicating the influence of climate and source rock lithology and their detrital origin. The upper part of the sequence, Coniacian-Maastrichtian (Fig. 2) shows the intercalation of marlstones and limestones in the detrital layers related to the variation of sedimentation conditions (Njike et al. 2014).

- **Rio-del-Rey sub-basin**

X-ray diffraction in the Cenomanian samples (MK1, MK2, MK6) exibits clays (illite, chlorite, vermiculite and kaolinite), and carbonates (calcite and dolomite). Calcite and dolomite could. Dolomite is related to the circulation of restricted marine pore waters near the mixing zone or may indicate elevated temperature and pressure conditions during diagenesis (Eyong 2003). The gradual decreases of clays (illite, chlorite and kaolinite) and carbonates (calcite and dolomite) from bottom to the top of the three samples could indicate that they are linked to the same genetic event, probably the sea level change, but this remains hypothetic as only three samples were collected with a wide spacing.

In the Campanian-Maastrichtian samples (DKA, DK1N and DK1B), kaolinite is also present but rather increase from bottom to the top in the sequence, with very high (dominant) siderite (Fe_2CO_3) in the basal sample (DK1A), not reported in other samples, indicating probably the sea level increasing that has led to reducing condition needed for deposition of siderite. Meanwhile, the siderite formation is indicative of a late diagenetic phenomenon, with calcite as precursor. It is reported in varied environments (Pye et al. 1990; Eyong 2003). The increase of kaolinite in this sequence is probably linked to the continental input during the sea level decrease.

5.6. Tectonic setting

The major-elements based discrimination plots of Verma and Armstrong-Altring (2013) were used to characterize the tectonic setting. These diagrams (Fig. 16A and 16B) have been widely and successfully used (Guadagnin et al. 2015; Nagarajan et al. 2015; Tawfick et al. 2017; Zaid 2015; Zeng et al. 2019; Tchouatcha et al. 2021) and discriminate three tectonic types (Arc-Rift-Collision) of two sets of low-silica rocks [(SiO_2)adj = 35–63%] and high-silica rocks [(SiO_2)adj = 63–95%]. All the plotted samples from the three sub-basins belong to the collisional tectonic setting with high-silica contents. Only one sample is out of the collisional tectonic setting and has low-silica content. Some recent work in the Logbadjeck Formation of the Douala sub-basin led to a similar interpretation (Ngueutchoua et al. 2019). In the Th-Sc-Zr/10 ternary plot (Fig. 16C and 16D) of Bhatia and Crook (1986), our samples correspond mainly to the continental island and passive continental margins and a few samples in the active continental margin (i.e. Campo samples in continental island arc, Douala samples in the continental island arc and passive continental margin, some in the active continental margin, and Rio-del-Rey samples in the continental island arc and passive continental margin). These results are similar to those of Ngueutchoua et al. (2019) corresponding to active and passive continental margins. According to a recent study in the northern part of the Douala sub-basin (Esue et al. 2021) most of the samples belong to the passive margin tectonic and others in the active continental margin or oceanic island arc.

All these results may indicate the complexity of the setting up of the Atlantic Basin of Cameroon. The Atlantic Basin of Cameroon is formed in a rift and passive tectonic context (Nguene et al. 1992; Njike Ngaha and Eno Belinga 1987; Ntamak-Nida et al. 2010; Njike Ngaha et al. 2014) (Fig. 19). Meanwhile, outcrops from the Campo sub-basin were affected by both normal and inverse faults, indicating respective distensional and compressional movements. Thus, if the geological history of the Atlantic Basin of Cameroon corresponds to passive and rifting settings, its evolution is marked by periods of compressional events, and the collision or active tectonic setting may reflect, on the one hand, the compressional events due to the filling pressure of sediments during the evolution of South Atlantic Ocean, and in the other hand, reflects the Precambrian basement history which experienced the Neoproterozoic orogeny (Nzenti et al. 1994; Toteu et al. 2001; Kroner and Stern 2004). Similar interpretations were made in numerous studies, such as in Recent deposits (e.g. Armstrong et al. 2015), Tertiary to Cretaceous (e.g. Tchouatcha et al. 2021) and Cretaceous deposits (Ngueutchoua et al. 2019a; Tchouatcha et al. 2021). The paleogeographic evolution of the Cameroon Atlantic Basin is given in Fig. 17. Anyway, it makes sense that after the morphological flattening of the Precambrian reliefs during the Proterozoic, great quantities of sediments were produced until the end of the proto-Atlantic rifting. This latter caused differential subsidence by reactivation of normal and antithetic rifting faults. In this context, the listric and reverse faults, well developed in the Campo sub-basin, indicate respectively syn-tectonic deposits periodically affected by compressional events.

5.7. Paleoenvironment and Paleogeographic evolution

- **Late Jurassic to Early Cretaceous**

This period corresponds probably to the second episode in the breakup of Pangea and South Atlantic Opening linked to the separation of African and South American Continents (Fig. 17A) associated with intense igneous activities (Scotese 2001; Njike Ngaha 1984; Njike Ngaha et al. 2014).

This opening led to the first detrital deposits in the Atlantic Basin, well known in the Campo sub-basin. These deposits are made up of alternated polygenic breccias interbedded with sandstones and/ or siltstones to claystones upward indicating gravity and rhythmic deposits. The facies and geochemical characteristics (Fig. 14A and B) indicate deep environments, probably in a lacustrine landscape with periodically marine incursion (Fig. 17B) as suggested by the exclusive continental palynomorph species such as *Classopollis* sp. and *Ephedripites* sp., and periodic formation of dolomite (Fig. 8C) linked probably by sea water incursions, under arid and semi-arid climate (Fig. 14C). The main sedimentary succession is characterized by a major retrogradation/progradation cycle with a well-developed progradational trend (Ntamak-Nida et al. 2010). The presence of listric and reverse faults (Fig. 3B and C) should have generated relative fluctuations in lake level and sediment supply due to the active faults creating alternative up- and down-lifting of basement blocs.

- **Middle to Late Cretaceous**

According to Seiglié et al. 1982, two sedimentary cycles are globally identified in the Douala sub-basin from Middle to Late Cretaceous, one cycle of low amplitude from Cenomanian to Turonian-Coniacian boundary, and the other one of hight amplitude from Turonian-Coniacian boundary to Late Maastrichtian.

The Cenomanian deposits (Lower to Middle Cenomanian) in the Douala sub-basin are mainly terrigenous made up essentially of sandstones and conglomeratic sandstones with interbedded clays indicating a rhythmic succession in a narrow rift and characteristic of deltaic environments (Njike Ngaha et al. 2014; Tchouatcha et al. 2021).

Several synthetic and antithetic normal faults, related to the progressive E-W distension between South American and African plates isolated small successive depressions, followed by a progressive sea water infiltration and variation of sedimentation conditions from lagoonal-lacustrine (Njike Ngaha et al. 2014) to shallow marine conditions (Fig. 17C) confirmed by the presence of Microforaminiferal test linings and dinoflagellate cysts.

From Late Cenomanian to Turonian, there was a significant subsidence of the faulted basement (Fig. 17D) linked to the progressive widening of the rift, the collapse of the entire block initiated a rise in the marine transgression towards the Nord of the Douala sub-basin (Njike Ngaha et al. 2014) with confined and shallow sea areas. This type of environment prevailed also in the Rio-del-Rey sub-basin right up to the Coniacian period. This phase is widely dominated by fossiliferous rich calcareous shales or marlstones facies.

During the Late Cretaceous, abundant marine species (Dinoflagellate and foraminiferal species) in the Campanian-Maastrichtian shales of the Rio-del-Rey sub-basin are related to the sea level rise (deep neritic), whereas in the Douala sub-basin, there is variation from bathyal to low deep neritic domain with regressive sedimentation (Cael and Kim 1979). The climate is globally arid to semi-arid in the Rio-del-Rey sub-basin, and arid to semi-arid and periodical semi-humid in the Douala sub-basin during Middle to Late Cretaceous (Fig. 14C).

6. Conclusion

The Atlantic Basin of Cameroon is composed of three sub-basins, located from South to North by the Campo (with probably the oldest deposits), Douala and Rio-del-Rey sub-basins. The Cretaceous deposits of the Campo sub-basin are of Early Cretaceous age (probably Neocomian to Albian), while those of the Douala and Rio-del-Rey sub-basins are from Early Cretaceous to Maastrichtian.

Fine-grained studied facies consist mainly of Fe-shales and shales associated with some Fe-sands and arkoses to sub-arkoses in the Douala sub-basin; Fe-sands in the Rio-del-Rey sub-basin, and rare wackes in the Campo sub-basin. The facies are more diversified in color in the Douala sub-basin than those of the Campo and Rio-del-Rey sub-basins.

The sediments from the Campo sub-basin originated from intermediate compositional rocks, those of the Douala sub-basin from dominant felsic rocks in the northern part and of intermediate composition in the southern part, and those from the Rio-del-Rey sub-basin from dominant felsic rocks.

The sediments from the Douala sub-basin are globally mature, those of the Campo sub-basin are rather sub-mature, and those of the Rio-del-Rey sub-basin are sub-mature to mature.

The sediments from the Campo sub-basin were deposited under arid to semi-arid climatic conditions, while those from the Douala sub-basin were formed under semi-humid to semi-arid climatic conditions and those from the Rio-del-Rey sub-basin were deposited in semi-arid to semi-humid climatic conditions.

The deposits from the Campo sub-basin formed in a relatively deep lacustrine environment, those from the Douala sub-basin in a fluvial to shallow marine environment and those from the Rio-del-Rey sub-basin in a marginal to shallow marine environment.

Overall, the collisional tectonic setting corresponds to the Precambrian history of the basement (Neoproterozoic collisional events) from which the sediments of the Atlantic Basin are derived. Compressional tectonics during the evolution of the South Atlantic Ocean were also involved.

Although the Campo, Douala, and Rio-del-Rey sub-basins share the same setting-up story during the opening of the Atlantic Ocean, there are some spreads such as the degree of maturity of sediments, the lithology of rock sources, and the environment of sedimentation.

All Cretaceous sequences of the Rio-del-Rey sub-basin have been affected by marine influence, those of the Douala sub-basin are dominated by fluvio-deltaic environments and periodically influenced by marine incursions, and those of the Campo sub-basin are dominated by fluvio-lacustrine environments and probably with periodic weak marine incursions as a result of variations of relative sea level during this period. The diagenetic effects on the deposits also varied from one sub-basin to another related to tectonic and sea level changes.

Declarations

Acknowledgment

We gratefully acknowledge Prof. Amr Said Deaf (University of Assiut, Egypt) for the opportunities and facilities for Palynologic analysis, and Prof. Sylvestre Ganno (University of Yaoundé 1, Cameroon) for opportunities of geochemical analyses.

Funding sources

This research did not receive any specific grant from funding agencies in the public, commercial, or not-for-profit sectors.

References

1. Absar N, Sreenivas B (2015) Petrology and geochemistry of greywackes of the ~ 1.6 Ga Middle Aravalli Supergroup, northwest India: Evidence for active margin processes. Int Geol Rev 57: 134–158.
2. Adediran SA, Adegoke OS, Oshin IO (1991) The Continental sediments of the Nigerian coastal basins. J Afr Earth Sci 12: 79–84.
3. Afenzar A, Essamoud R (2018) Early Mesozoic detrital and evaporitic synrift series of the Mohammedia–Benslimane–El Gara–Berrechid basin (western Meseta, Morocco): sedimentary and palaeoenvironmental evolution and comparison with the basins of the northeastern American Margin. In Conjugate Margins Conferences – Abstracts. Atlantic Geol. 54: 409 – 407.
4. Alves TM, Tiago A, Cunha TA (2018) A stratigraphic record of enhanced subsidence during continental breakup: do breakup sequences rule over unconformities? In Conjugate Margins Conferences – Abstracts. Atlantic Geol 54: 409 – 407.
5. Anaya-Gregorio A, Armstrong-Altrin JS, Machain-Castillo ML, Montiel-García PC, Ramos-Vázquez MA (2018) Textural and geochemical characteristics of late Pleistocene to Holocene fine-grained deep-sea sediment cores (GM6 and GM7), recovered from southwestern Gulf of Mexico. J. Palaeogeogr 7: 253–271.
6. Andreef I (1947) Etude du bassin sédimentaire de Campo. Rapport interne, Elf, Serepca, p 58
7. Armstrong-Altrin JS, Nagarajan R, Madhavaraju J, Rosalez-Hoz L, Lee YI, Balaram V, Cruz-Martinez A, Avila-Ramirez G (2013) Geochemistry of Jurassic and Upper Cretaceous shales from the Molango Region, Hildago, eastern Mexico: implications for source-area weathering, provenance, and tectonic setting. Compt Rendus Geosci 345: 185–202.

8. Armstrong-Altrin JS, Nagarajan R, Balaram V, Natalhy-Pineda O (2015) Petrography and geochemistry of sand from the Chachalacas and Veracruz beach areas, western Gulf of Mexico, Mexico: constraints on provenance and tectonic setting. J. South Amer Earth Sci 64: 199–216.
9. Ashukem EN, Bisse SB, Philip F, Bokanda EE, Ngo Maih Bahoya MP, Tsamnye JJ, Tonye MD, Belinga Belinga C, Yugye JA, Ekomane E (2022) Petrography and geochemistry of sandstones in the Kribi-Campo sub-basin (South Cameroon): implications for diagenetic evolution and provenance. Arab J Geosci 15: 295.
10. Bau M, Dulski P (1996) Distribution of yttrium and rare-earth elements in the Penge and Kuruman iron-formations, Transvaal 496 Supergroup, South Africa. Precambrian Res 79: 37–55.
11. Belmonte YC (1966) Stratigraphie du bassin sédimentaire du Cameroun. In: Proceeding of the 2nd West African Micropaleontologist Colloquium, Ibadan, Nigeria, pp 7–23.
12. Benkhelil J, Giresse P, Poumot C, Ngueutchoua G (2002) Lithostratigraphic, geophysical, and morpho-tectonic studies of the South Cameroon shelf. Mar Petrol Geol 19: 499–517
13. Bessa Ekoa, A.Z., Ndjigui P. D., Fuh G.C., Armstrong-Altrin J.S., Betsi Bineli, T., 2021. Mineralogy and geochemistry of the Ossa Lake Complex sediments, Southern Cameroon: implications for paleoweathering and provenance. Arabian Journal of Geosciences 14, 322
14. Bhatia MR, Crook KA 1986 Trace element characteristics of greywackes and tectonic setting discrimination of sedimentary basins. Contrib Mineral Petrol 92: 181–193.
15. Blatt H, Middleton GV, Murray R (1972) Origin of sedimentary rocks. Englandwood Cliff, New Jersey, Prentice Hall, p 634
16. Boboye OA, Okon EE (2014) Sedimentological and geochemical characterization of the Cretaceous strata of Calabar flank, southeastern Nigeria. J Afri Earth Sci 99: 427–441.
17. Boltenhagen E (1976) Pollens et spores sénoniens du Gabon. Cahiers de Micropaléontologie, 3, p 21
18. Cao J, Wu M, Chen Y, Hu K, Bian LZ, Wang LG, Zhang Y (2012) Trace and rare earth element geochemistry of Jurassic mudstones in the northern Qaidam Basin, northwest China. Chem der Erde 72: 245–252.
19. Chen A, Jin C, Lou Z, Chen H, Xu S, Huang K, Hu S (2013) Salt Tectonics and Basin Evolution in the Gabon Coastal Basin, West Africa. J. Earth Sci 24: 903–917.
20. Chevalier C (1982) Bassin de Campo: compte rendu de mission de terrain. Rapport interne Elf-Serepca, p 32
21. Cox R, Low DR, Culler RL (1995) The influence of sediment recycling and basement composition on evolution of mudrock chemistry in the Southwestern United States. Geochem Cosmochim Acta 59: 2919–2940.
22. Cullers RL, Podkovyrov VN (2000) Geochemistry of the Mesoproterozoic Lakhanda shales in Southeastern Yakutia, Russia: Implications for Mineralogical and Provenance Control, and Recycling. Precambrian Res 104: 77–93

23. De Ros LF, Mizusaki AMP, Silva CMA, Anjos SMC (2003) Volcanic rock fragments of Paraná Basin provenance in the Upper Cretaceous sandstones of Santos Basin, Eastern Brazilian Margin. 2º Congresso Brasileiro De P&D Em Petróleo & Gás
24. Dowla N, Bird DE, Michael A, Murphy MA (2018) Full-fit reconstruction of the central Atlantic. In Conjugate Margins Conferences – Abstracts. Atlantic Geol 54: 409 – 407.
25. Dumort JC (1968) Carte géologique de reconnaissance du Cameroun à l'échelle 1/500 000, feuille Douala-Ouest, avec notice explicative. Imprimerie Nationale, Yaoundé, Cameroun, p 69
26. Dupré S, Bertotti G, Cloetingh S (2007) Tectonic history along the South Gabon Basin: Anomalous early post-rift subsidence. Mar Petroleum Geol 24: 151–172.
27. Dunoyer De Segonzac G (1970) The transformation of clay minerals during diagenesis and lower-grade metamorphism: A review. Sedimentol 15: 281–346.
28. Edet JJ, Nyong EE (1994) Palynostratigraphy of Nkporo shale exposures (Late Campanian-Maastrichtian) on the Calabar Flank, SE Nigeria. Rev Paleobot Palynol 80: 131–147.
29. Enu EI (1986) Influence of tectonics and palaeoenvironment on late Cretaceous clay sedimentation in the Upper Benue Trough, Nigeria. Geol J 21: 93–99.
30. Esue MF, Agyingi MC, Tendo FJ, Lordon EDA (2021) Geochemistry of carbonate-clastic strata in NW Douala sub-basin, Cameroon: Implications for provenance, tectonics and source area weathering. J Sed Environment 6: 57–71.
31. Eyong, J.T., 2003. Litho-Biostratigraphy of the Mamfe Cretaceous Basin, S.W. Province of Cameroon-West Africa. PhD Thesis. University of Leeds, UK, p 265
32. Fedo CM, Nesbitt HW, Young GM (1995) Unravelling the Effects of Potassium Metasomatism in Sedimentary Rocks and Paleosols, with Implications for Paleoweathering Conditions and Provenance. Geol 23: 921–924.
33. Floyd PA, Leveridge BE (1987) Tectonic environments of the Devonian Gramscatho Basin. South Cornwall: framework mode and geochemical evidence from turbidite sandstones. J Geol Soc Lond 144: 531–542.
34. Garzanti E, Padoan M, Setti M, Lopez-Galindo A, Villa IM (2014) Provenance versus weathering control on the composition of tropical river mud (Southern Africa). Chem Geol 366: 61–74.
35. Garzanti E, Vezzoli G, Ando S, Limonta M, Borromeo L, Francelanord C (2019) Provenance of Bengal shelf sediments: 2. Petrology and Geochemistry of sand. J Mineral 9: 642.
36. Goode JK, Belopolsky A, Grow T, Whitehouse P (2018) Sergipe–Alagoas Basin, eastern Brazilian margin – oblique rifting with an igneous overprint. In Conjugate Margins Conferences – Abstracts. Atlantic Geol 54: 409 – 407.
37. Guadagnin F, Junior FC, Magalhaes AJC, Alessandretti L, Ballico MB, Jelinek AR (2015) Sedimentary petrology and detrital zircon U–Pb and Lu–Hf constraints of Mesoproterozoic intracratonic sequences in the Espinhaço Supergroup: Implications for the Archean and Proterozoic evolution of the São Francisco Craton. Precambrian Res 266: 227–245.

38. Hayashi KI, Fujisawa H, Holland HD, Ohmoto H (1997) Geochemistry of 1.9 Ga Sedimentary Rocks from Northeastern Labrador, Canada. Geochem Cosmochim Acta 61: 4115–4137.
39. Hernández-Hinojosa V, Montiel-García P.C., Armstrong-Altrin J.S., Nagarajan R., Kasper-Zubillaga J.J., 2018. Textural and geochemical characteristics of beach sands along the western Gulf of Mexico, Mexico. Carpathian Journal of Earth Environmental Sciences 13, 161–174
40. Herron MM (1988) Geochemical classification of terrigenous sands and shales from core or log data. J Sed Petrol 58: 820–829.
41. Hossain I, Roy KK, Biswas PK, Alam M, Moniruzzaman Md, Deeba F (2014) Geochemical Characteristics of Holocene Sediments from Chuadanga District, Bangladesh: Implications for Weathering, Climate, Redox Conditions, Provenance and Tectonic Setting. Chin J Geochem 33: 336–350.
42. Jones, B., Manning, D.A.C., 1994. Comparison of geochemical indices used for the interpretation of palaeoredox conditions in ancient mudstones. Chemical Geology 111, 111–129.
43. Kenfack PL, Njike Ngaha PR, Ekodeck, GE, Ngueutchoua, G (2012) Fossils dinoflagellates from the northern border of the Douala sedimentary sub-basin (South-West Cameroon): Age assessment and paleoecological interpretations. Geosci 2: 117–124
44. Kröner A, Stern RJ (2004) Pan-African Orogeny, vol. 1. Elsevier, Amsterdam, pp 1–12.
45. Kurobasa A, Davison I, Doran H (2018) Correlating the Albian magmatic rift across the Sergipe–Alagoas and North Gabon conjugate margin: implications for source rocks above SDRs. In Conjugate Margins Conferences – Abstracts. Atlantic Geol 54: 409 – 407.
46. Liu R, Liu ZJ, Sun PC, Xu YB, Liu DQ, Yang XH, Zhang C (2015) Geochemistry of the Eocene Jijuntun Formation oil shale in the Fushun Basin, northeast China: Implications for source-area weathering, provenance and tectonic setting. Chem der Erde 75: 105–116.
47. Lowe DR (1982) Sediment gravity flows: II. Depositional models with special reference to the deposits of high-density turbidity currents. J Sed Petrol 52: 279–297.
48. Ma PF, Wang LC, Wang CS, Wu XH, Wei YS (2015) Organic matter accumulation of the lacustrine Lunpola oil shale, central Tibetan Plateau: controlled by the paleoclimate, provenance, and drainage system. Int J Coal Geol 147:148, 58–70
49. Madukwe HY, Obasi RA (2015) Classification maturity, provenance, tectonic setting and source-area weathering of the Ilubirin stream sediments, South-West, Nigeria. Int J Sci 4: 7–21.
50. Mahmoud, M.S., 2000. Plio-Pleistocene palynology (freshwater algae, spores and pollens) and palaeoecology of the shallow subsurface section, West Assiut, Egypt. Acta University of Carolina 44, 101–114.
51. Mbesse CO, Roche E, Ngos III S (2012) La limite Paleocene-Eocene dans le bassin de Douala (Cameroun). Biostratigraphie et essai de reconstitution des paléoenvironnements par l'étude des dinoflagellés. Geo-Eco-Trop 36: 83–119.
52. McDonough WF, Sun SS (1995) The Composition of the Earth. Chemical Geology 120: 223–253.

53. McLennan SM (2001) Relationships between the Trace Element Compositions of Sedimentary Rocks and Upper Continental Crust. Geochemistry, Geophys Geosyst 2: 86–98.
54. Meng Q T, Liu ZJ, Bruch AA, Liu R, Hu F (2012) Palaeoclimatic evolution during the Eocene and its influence on oil shale mineralisation, Fushun Basin, China. J Asi Earth Sci 45: 95–105.
55. Miall AD (1996) The Geology of Fluvial Deposits: Sedimentary Facies, Basin Analysis, and Petroleum Geology. Springer-Verlag. p 582
56. Mongelli G, Critelli S, Perri F, Sonnino M, Perrone V (2006) Sedimentary Recycling, Provenance and Paleoweathering from Chemistry and Mineralogy of Mesozoic Continental Redbed Mudrocks, Peloritani Mountains, Southern Italy. Geochem J 40: 197–209.
57. Moradi AV, Sarı A, Akkaya P (2016) Geochemistry of the Miocene oil shale (Hançili Formation) in the Çankırı-Çorum Basin, Central Turkey: Implications for Paleoclimate conditions, source-area weathering, provenance and tectonic setting. Sed Geol 341: 289–303.
58. Mortazavi M, Moussavi-Harami R, Mahboubi A, Nadjafı M (2014) Geochemistry of the Late Jurassic–Early Cretaceous shales (Shurijeh Formation) in the intracontinental Kopet Dagh Basin, northeastern Iran: implication for provenance, source weathering, and paleoenvironments. Arab J Geosci 7: 5353–5366.
59. Nagarajan R, Armstrong-Altrin JS, Kessler FL, Hidalgo-Moral EL, Dodge Wan D, Taib NI (2015) Provenance and Tectonic Setting of Miocene Siliciclastic Sediments, Sibuti Formation, Northwestern Borneo. Arab J Geosci 8: 8549–8565.
60. Nesbitt HW, Young GM (1982) Early Proterozoic Climates and Plate Motions Inferred from Major Element Chemistry of Lutites. Nat 299:715–717.
61. Nesbitt HW, Young GM (1984 Prediction of Some Weathering Trend of Plutonic and Volcanic Rocks Based on Thermodynamic and Kinetic Consideration. Geochem Cosmochim Acta 48:1523–1534.
62. Nguene FR, Tamfu SF, Loule JP, Ngassa C (1992) Paleoenvironment of the Douala and Kribi/Campo sub-basins, in Cameroon, West Africa. Explor Product Elf Aquitaine, 13: 129–139.
63. Ngueutchoua G, Ngantchu LD, Youbi M, Ngos III S, Beyala VKK, Yifomju KP, Tchamgoué JC (2017) Geochemistry of Cretaceous mudrocks and sandstones from Douala sub-basin, Kumba area, southwest Cameroon: constraints on provenance, source rock weathering, paleo-oxidation conditions and tectonic environment. Int J Geosci 8: 393–424.
64. Ngueutchoua G, Ekoa Bessa AZ, Eyong Takem J, Demanou Zandjio D, Djaoro Baba H, Tchami Nfada L (2019a) Geochemistry of cretaceous fine-grained siliciclastic rocks from Upper Mundeck and Logbadjeck formations, Douala sub-basin, SW Cameroon: Implications for weathering intensity, provenance, paleoclimate, redox-condition, and tectonic setting. J Afr Earth Sci 152: 215–236.
65. Ngueutchoua G, Eyong Takem J, Ekoa Bessa AZ, Agheenwi Azanji ZB, Maschouer Emane A, Kemteu Sobdjou C, Dzoti Lontchi Y, Hamadou T, Baboule Ongbassouek BM, Nguemo Kenfack GR (2019b) Provenance and depositional history of Mesozoic sediments from the Mamfe basin and Douala sub-basin (SW Cameroon) unraveled by geochemical analysis. J Afr Earth Sci 158: 103550.

66. Njike Ngaha PR (1984) Contribution à l'étude géologique, stratigraphique et structurale de la bordure du bassin atlantique au Cameroun. Thèse de 3ème cycle, Université de Yaoundé, p 131
67. Njiké Ngaha PR, Eno Belinga SM (1987) Le diachronisme du « grès de base », le paléoenvironnement et le rôle de l'ouverture de l'Atlantique sud. Ann Fac Sci Terre 4: 113–119.
68. Njike Ngaha PR. (2005) Palynostratigraphie et reconstitution des paléoenvironnements du Crétacé de l'Est du bassin sédimentaire de Douala (Cameroun). Thèse d'État, Université de Yaoundé I, p 259
69. Njike Ngaha PR, Mfayakouo CB, Bitom D (2014) Paleogeographic Evolution of the Eastern Edge of the Douala Basin from Early Cenomanian to Turonian. Open Geol J 8: 124–141.
70. Njoh AO, Bassey EA, Essien AJ, Agbor VW (2013) Palynostratigraphy of Early Cretaceous sedimentary deposits from the Rio del Rey Basin S.W. Cameroon. J Camer Acad Sci 11: 63–73.
71. Njoh AO, Victor O, Christopher A (2013) Campano-Maastrichtian foraminifera from onshore sediments in the Rio del Rey Basin, Southwest Cameroon. J Afr Earth Sci 79: 157–164.
72. Njoh AO, Essien J, Ama TA (2014) Albian-Turonian palynomorphs from Mundeck and Logbadjeck Formations, Ediki River, North-western part of the Douala sub-basin, Cameroon. Sci Technol Develop 15: 66–77.
73. Njoh AO, Taku JA (2016) Shallow marine Cretaceous sequences and petroleum geology of the onshore portion Rio del Rey Basin, Cameroon, Gulf of Guinea. Open J Mar Sci 6: 177–192.
74. Njoh AO, Mbanda LN, Ngoe DE (2018) Cretaceous-Tertiary Foraminifera and Palynomorphs from Djega section and inferred paleodepositional environments, Rio del Rey Basin, Cameroon, West Africa. Scientific World J 1–9.
75. Ntamak-Nida MJ, Baudin F, Schnyder J, Makong JC, Komguem PB, Abolo GM (2008) Depositional environments and characterization of the organic matter of the Lower Mundeck Formation (Barremian?–Aptian) of the KribiCampo sub-basin (South Cameroon): implications for petroleum exploration. J Afr Earth Sci 51: 207–219.
76. Ntamak-Nida MJ, Bourquin S, Makong JC, Baudin F, Mpesse JE, Itjoko Ngouem C, Komguem PB, Abolo GM (2010) Sedimentology and sequence stratigraphy from outcrops of the Kribi-Campo sub-basin: Lower Mundeck Formation (Lower Cretaceous, southern Cameroon). J Afri Earth Sci 58: 1–18.
77. Nzenti JP, Barbey P, Bertrand JM, Macaudière J (1994) La Chaîne panafricaine au Cameroun: Cherchons suture et modèle ! In : SGF édit. 15e Réunion des Sciences de la Terre, Nancy, France, p 99
78. Oyebanjo O, Bukalo N, Ekosse GI (2021) Provenance and Paleoenvironmental Studies of Cretaceous African and South American Kaolins: Similarities and Differences. Minerals 11: 1074.
79. Perri F, Critelli S, Mongelli G, Cullers RL (2011) Sedimentary Evolution of the Mesozoic Continental Redbeds Using Geochemical and Mineralogical Tools: The Case of Upper Triassic to Lowermost Jurassic Monte di Gioiosa Mudrocks (Sicily, Southern Italy). Int J Earth Sci 100: 1569–1587.
80. Pye K, Dickson JAD, Schiavon N, Coleman ML, Cox M (1990) Formation of siderite-Mg-calcite-iron sulphide concretionin in intertidal marsh and sandflat sediments, north Norfolk, England. Sedimentol 37: 325–343.

81. Rao W, Tan H, Jiang S, Chen J (2011) Trace element and REE geochemistry of fine- and coarse-grained sands in the Ordos deserts and links with sediments in surrounding areas. Chem der Erde 71: 155–170.
82. Regnoult JM (1986) Synthèse géologique du Cameroun. République du Cameroun, Ministère des Mines et de l'Énergie, Direction des Mines et de la Géologie, p 119.
83. Reyre D (1959) Bassins sédimentaires côtiers. In: Notice explicative sur la feuille Yaoundé-Ouest, carte géologique de reconnaissance à l'échelle 1/500 000 par G. Champetier de Ribes et D. Reyre, 1–14.
84. Roser BP, Korsch RJ (1988) Provenance signatures of sandstone-mudstone suites determined using discriminant function analysis of major-element data. Chem Geol 67: 119–139.
85. Salard-Cheboldaeff M (1977) Palynologie du bassin sédimentaire Littoral du Cameroun dans ses rapports avec la stratigraphie et la paléoécologie. Ph.D thesis, University of Pierre et Marie Curie, France, p 262
86. Salard-Cheboldaeff M (1978) Palynoflore maestrichtienne et tertiaire du bassin sédimentaire littoral du Cameroun, Pollen et spores. Musée National d'Histoire Naturelle, 215 – 26 0
87. Salard-Cheboldaeff M (1979) Palynologie Maestrichtienne et Tertiaire du Cameroun. Etude qualitative et répartition verticale des principales espèces. Rev Palaeobot Palynol 365–388.
88. Salard-Cheboldaeff M (1981) Palynologie Maestrichtienne et Tertiaire du Cameroun. Résultats Botaniques. Rev Palaeobot Palynol 32: 401–439.
89. Scotese CR (2001) Atlas of Earth History. Paleogeography, PALEO-MAP Project, Texas, 1: 1–52.
90. Shi ZS, Chen KY, Shi J, Liu BJ, He HJ, Liu G (1994) Feasibility analysis of the application of the ratio of strontium to barium on the identifying sedimentary environment. Fault-Block Oil Gas Field 10: 12–16.
91. Singer A (1988) Illite in aridic soils, desert dusts and desert loess. Sed Geol 59: 251–259.
92. Suttner LJ, Dutta PK (1986) Alluvial sandstone composition and paleoclimate, I, Framework mineralogy. J Sed Petrol 56: 329–345.
93. Tao H, Wang Q, Yang X, Jiang L (2013) Provenance and tectonic setting of Late Carboniferous clastic rocks in West Junggar, Xinjiang, China: A case from the Hala-alat Mountains. J Asi Earth Sci 64: 210–222.
94. Tawfik HA, Salah MK, Maejima W, Armstrong-Altrin JS, Abdel-Hameed AMT, El Ghandour MM (2017) Petrography and geochemistry of the Lower Miocene Moghra sandstones, Qattara Depression, Northwestern Desert, Egypt. Geol J 1–16.
95. Taylor SR, McLennan SM (1985) The Continental Crust: its Composition and Evolution. Blackwell Scientific, Oxford, p 312
96. Tchouatcha MS (2005) Étude sédimentologique de quelques facies sableux crétacés du secteur oriental du bassin de Douala: genèse et signification paléoenvironnementale. Mém. D.E.A., University of Yaoundé 1, Cameroun, p 101

97. Tchouatcha, M.S., Kassi Kassi, P., Mbesse, C.O., Kuété Noupa, R., Mam, W.J., Préat, A., (2022) Geochemistry of onshore deposits from Rio-del-Rey sub-basin of the western Atlantic margin of Cameroon (Coastal basin, South-West Cameroon): Provenance and environments of sedimentation. Environmental Earth Sci 81: 321
98. Tchouatcha MS, Kouske AP, Deaf AS, Mioumnde AP (2021a) Geochemical, mineralogical and sedimentological analyses of reworked sediments (new) in the syn- to post-rift Middle Cretaceous-Quaternary detrital deposits from western Atlantic margin of Cameroon: evidence from sedimentation-erosion alternation in the context of passive margin evolution. Acta Geochim 40(5): 676–701.
99. Tchouatcha MS, Tamfuh Azinwi P, Kemteu Sobdjou C, Mbesse CO, Ngnotue T (2021b) Provenance, palaeoweathering and depositional environment of the Cretaceous deposits from the Babouri-Figuil and Mayo Oulo-Lere basins (North-Cameroon) during the Southern Atlantic opening: Geochemical constraints. J. Afr. Earth Sci. 174.
100. Teisserenc P, Villemin J (1989) "Sedimentary Basin of Gabon—Geology and Oil Systems", Divergent/Passive Margin Basins, J. D. Edwards, P. A. Santogrossi
101. Toteu SF, Van Schmus RW, Penaye J, Michard A (2001) New U–Pb and Sm–Nd data from north-central Cameroon and its bearing on the pre-Pan-African history of central Africa. Precambrian Res 108: 45–73.
102. Valença LMM, Neumann VH, Mabesoone JM (2003) An overview on Callovian-Cenomanian intracratonic basins of Northeast Brazil: Onshore stratrigraphic record of the opening of the southern Atlantic. Geol Acta 1: 261–275.
103. Verma SP, Armstrong-Altrin JS (2013) New multi-dimensional diagrams for tectonic discrimination of siliciclastic sediments and their application to Pre-Cambrian basins. Chem Geol 355: 117–180.
104. Wang MF, Jiao YQ, Wang ZH, Yang Q, Yang SK (2005) Recovery paleo-salinity in sedimentary environment: an example of mudstone in Shuixigou group, southwestern margin of Turpan-Hami basin, Xin jiang. Petrol Geol 26: 719–722.
105. Zaid SM (2015) Geochemistry of sands along the Ain Soukhna and Ras Gharib beaches, Gulf of Suez, Egypt: Implications for provenance and tectonic setting. Arab J Geosci 8: 10481–10496.
106. Zeng S, Wang J, Chen W, Fu X, Feng X, Song C, Wang D, Sun W (2019) Geochemical characteristics of Early Cretaceous marine oil shale from Changshe Mountain area in the northern Qiangtang Basin, Tibet: Implication for palaeoweathering, provenance, tectonic setting, and organic matter accumulation. Geol J 1–18.
107. Zheng RC, Liu MQ (1999) Study on palaeosalinity of Chang-6 oil reservoir set in Ordos Basin. Oil and Gas Geol 20: 20–25.
108. Zhou L, Friis H, Poulsen MLK (2015) Geochemical evaluation of the Late Paleocene and Early Eocene shales in Siri Canyon, Danish-Norwegian Basin. Mar Petrol Geol 61: 111–122.
109. Regnoult JM 1986 Synthèse géologique du Cameroun. République du Cameroun, Ministère des Mines et de l’Énergie, Direction des Mines et de la Géologie, 119p.

Tables

Table 2 to 4 are available in supplementary file.

Figures

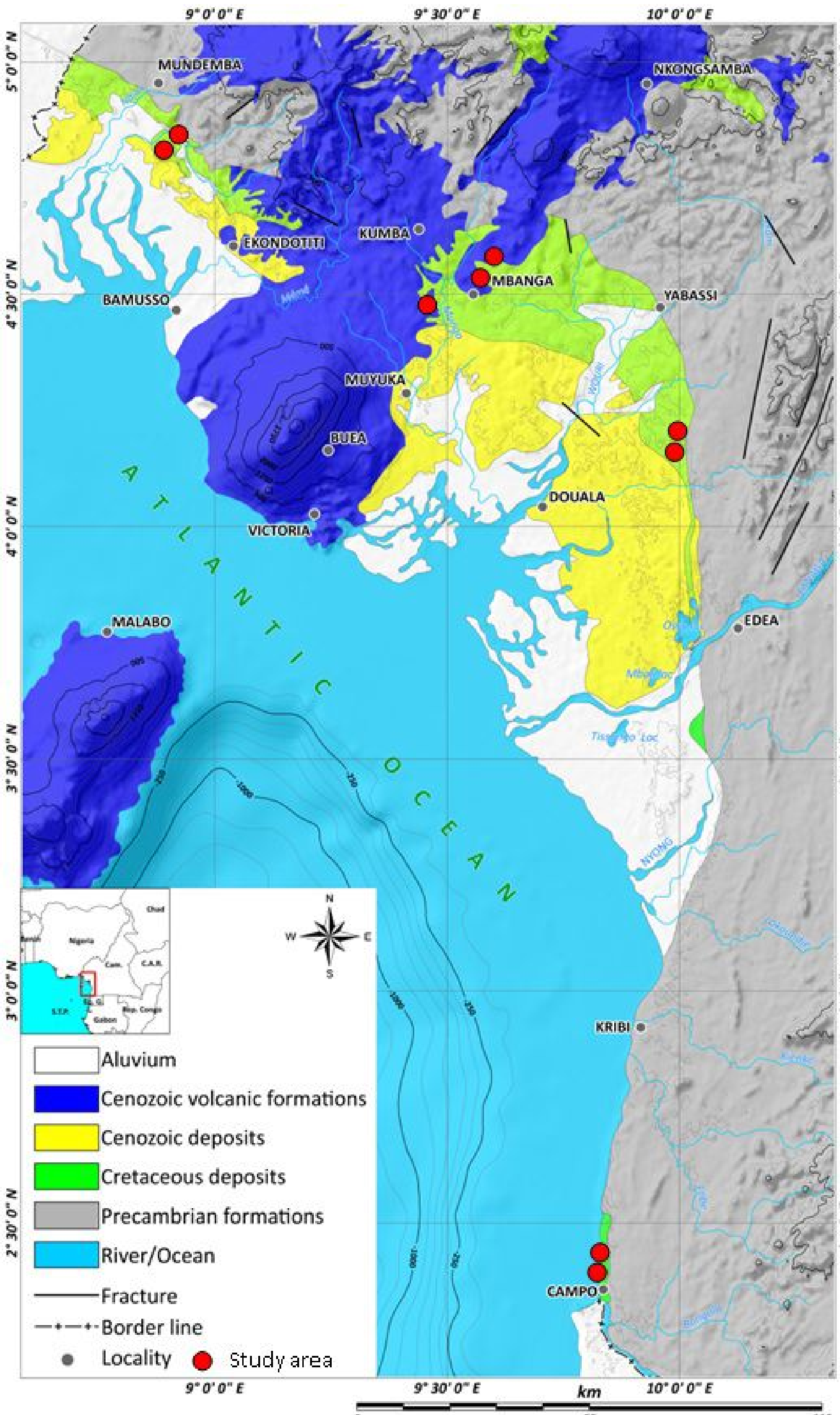

Figure 1

Geological map of the Atlantic Basin of Cameroon (Modified from Dumort, 1968; Njike Ngaha et al., 2014; Ntamak-Nida et al., 2010; Tchouatcha et al., 2021)

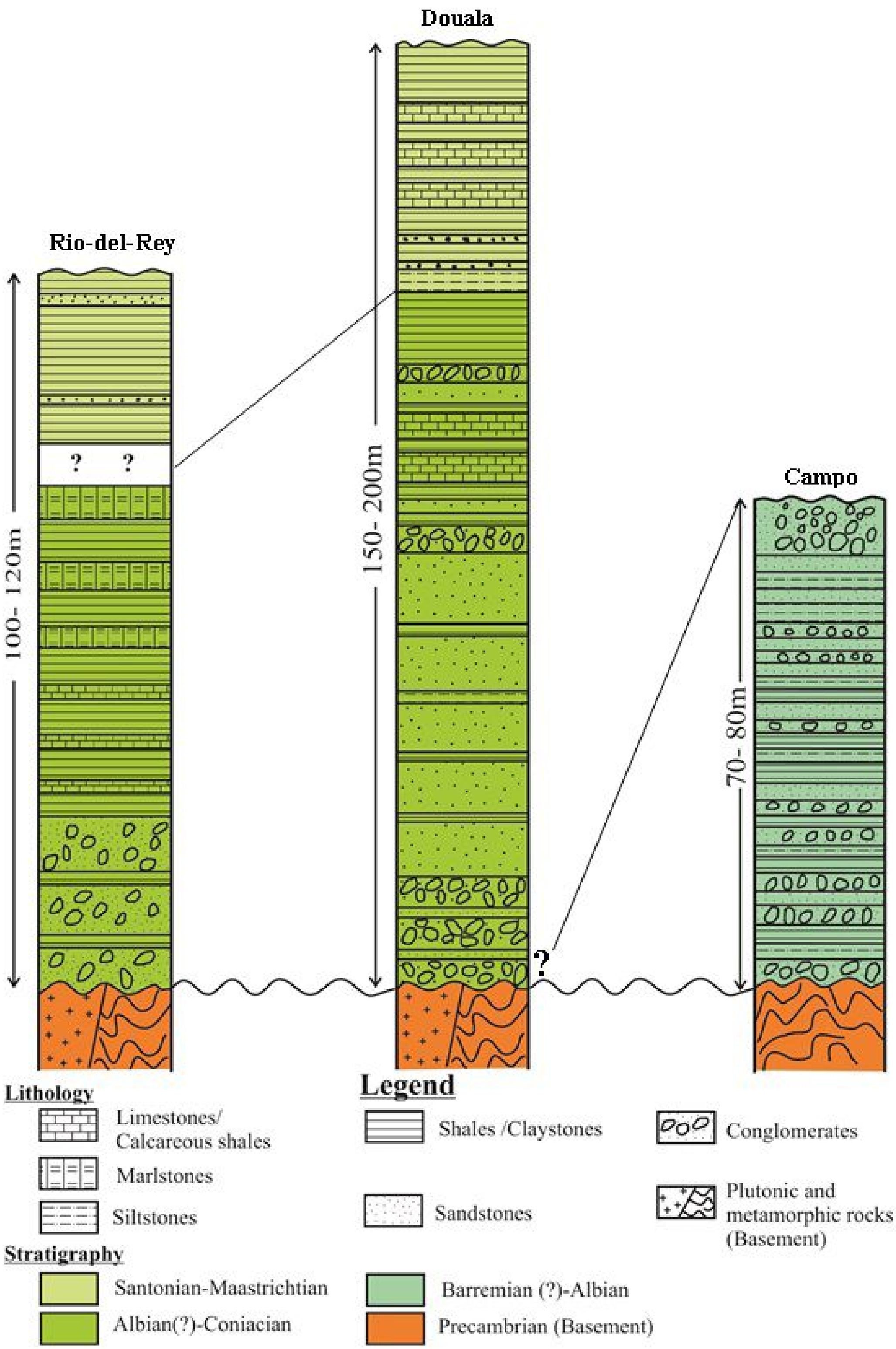

Figure 2

Synthetic logs of outcrops from the Rio-del-del-Rey sub-basin (A) (Modified from Njoh et al. 2018, Douala sub-basin (B) (Modified from Njike Ngaha, 2005; Njike Ngaha et al. 2014) and Campo sub-basin (C)

(Modified from Njike Ngaha and Eno Belinga, 1987; Ntamak-Nida et al. 2010).

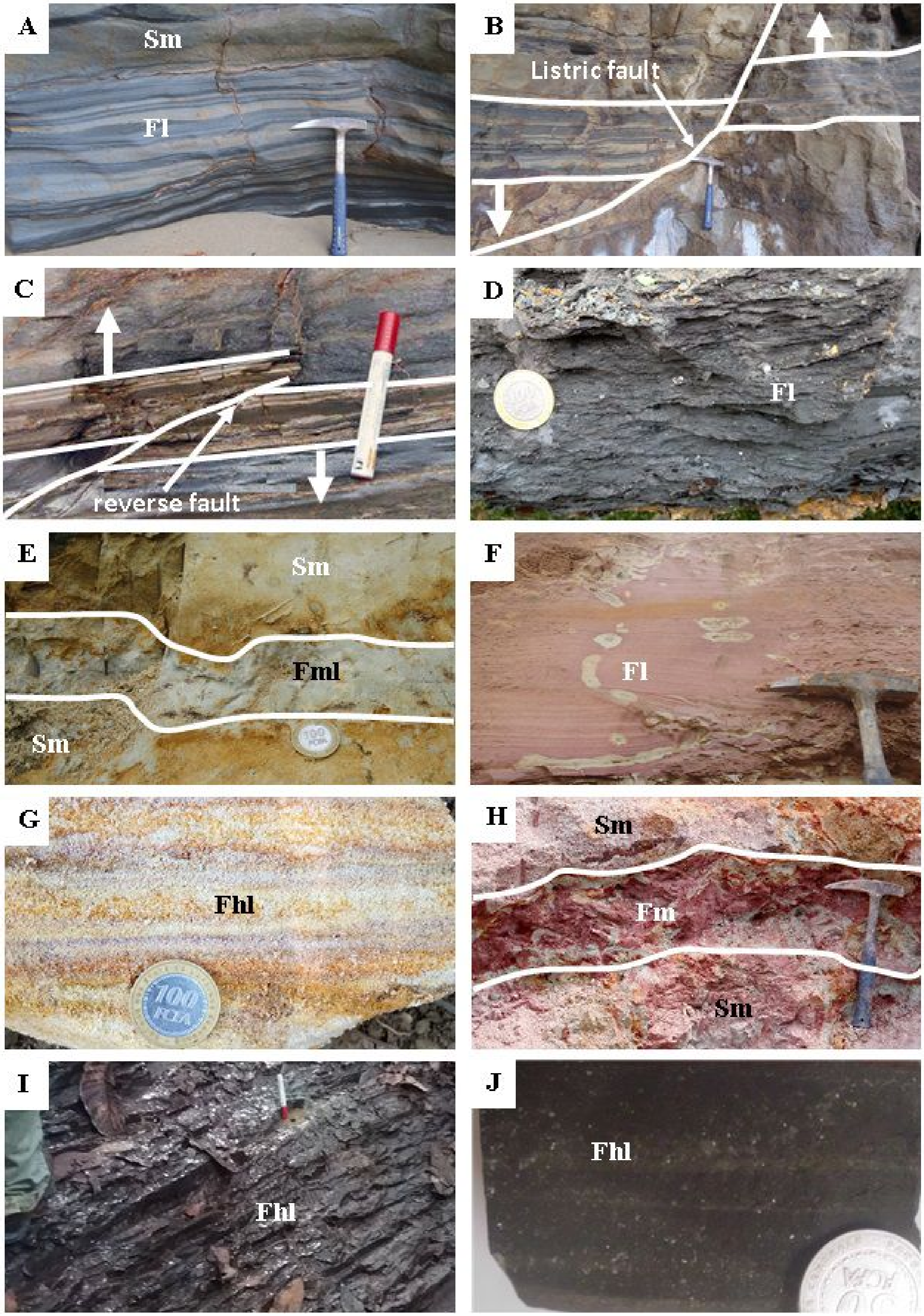

Figure 3

Field photographs of some outcrops and hand specimens from the Atlantic Basin: A: Rhythmic deposit with blackish shale (Fl) and greyish sandstone alternation; B: Listric fault affecting the deposits; C: Reverse fault affecting the deposits (Ntamak-Nida et al., 2010); D: Black clay with lamination (Fl); E: Greenish silts interbedded in sandstones; F: Reddish clay with lamination (Fl); G: Hand specimen of mottled (yellowish, grey, maroon and purple) and laminated sandy clay; H: Massive mottled (red and whitish grey) clay interbedded in sandstone; I: Hand specimen of mottled (green and red) massive clay; J: Hand specimen of laminated black calcareous shale. N.B.: A - C: from Campo sub-basin; D – H: from Douala sub-basin; I and J: from Rio del Rey sub-basin.

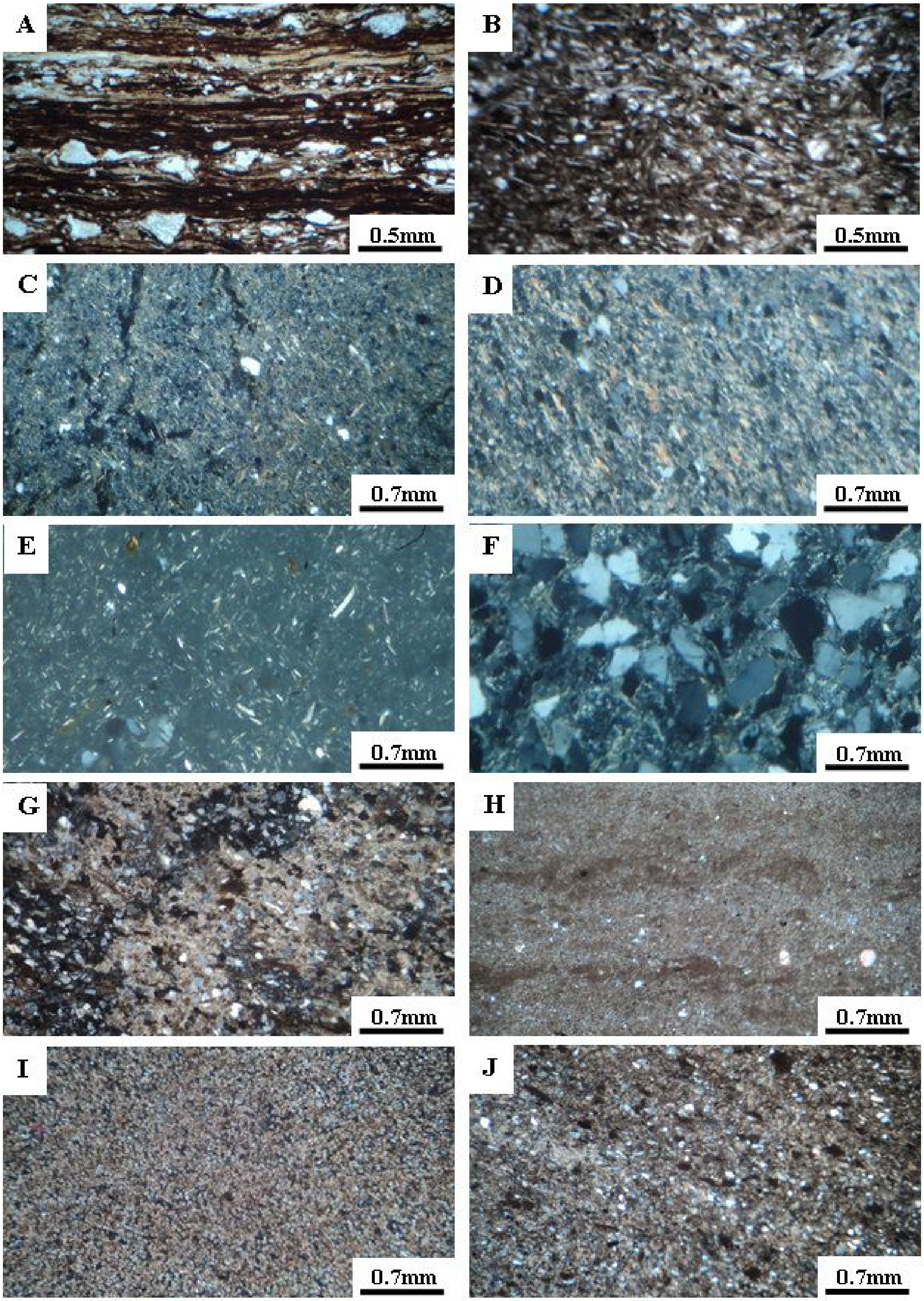

Figure 4

Microstructure photographs of the main facies from the Atlantic Basin: A, B and D: Very fine-grained clastic and isogranular microstructure; C: Cryptocristalline microstructure; E: Very fine-grained clastic isogranular microstructure; F and G: Fine-grained clastic and heterogranular microstructure; H: Fine-grained clastic isogranular microstructure; I: Fine-grained clastic heterogranular and laminated microstructure; J: Fine-grained clastic isogranular microstructure. N.B.: A and B: from Campo sub-basin; C – F: from Douala sub-basin; G – J: from Rio del Rey sub-basin.

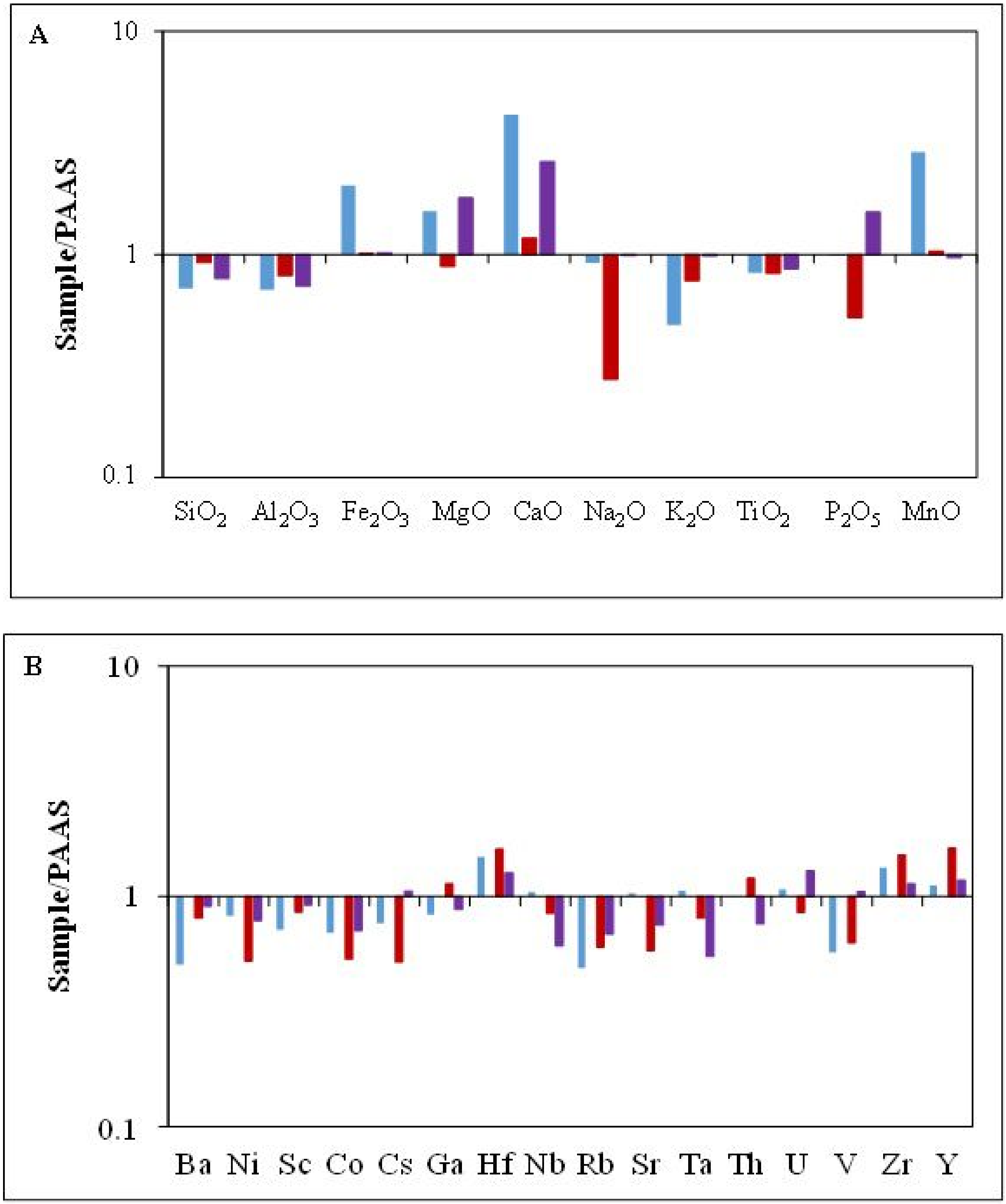

Figure 5

A: Stick diagram of average major elements and correlation between fine-grained deposits from Campo, Douala and Rio-del-Rey sub-basins; B: Stick diagram of average trace elements and correlation between fine-grained deposits from Campo, Douala and Rio-del-Rey sub-basins

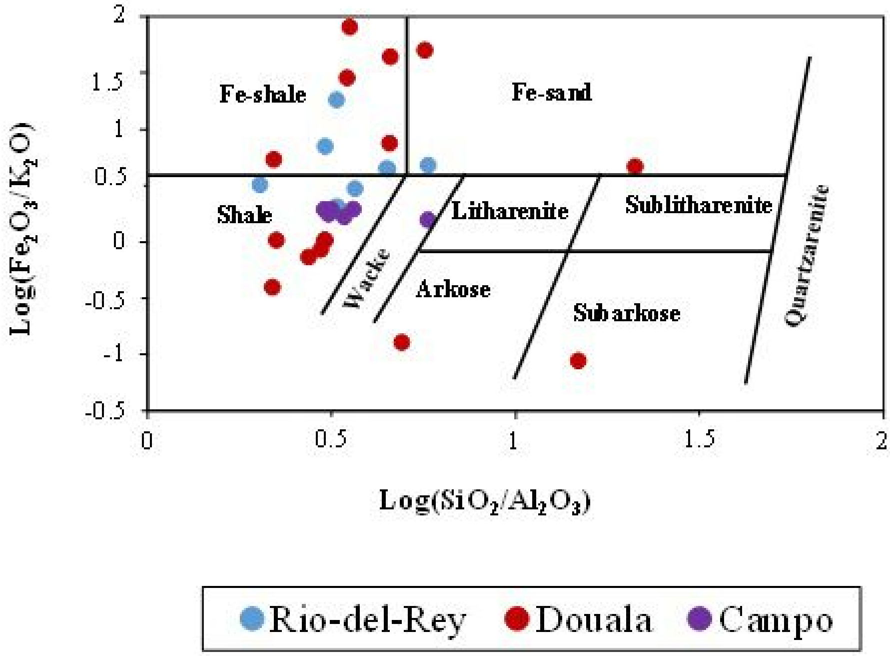

Figure 6

Classification of studied fine-grained deposits according to the scheme of Herron's (1988) diagram.

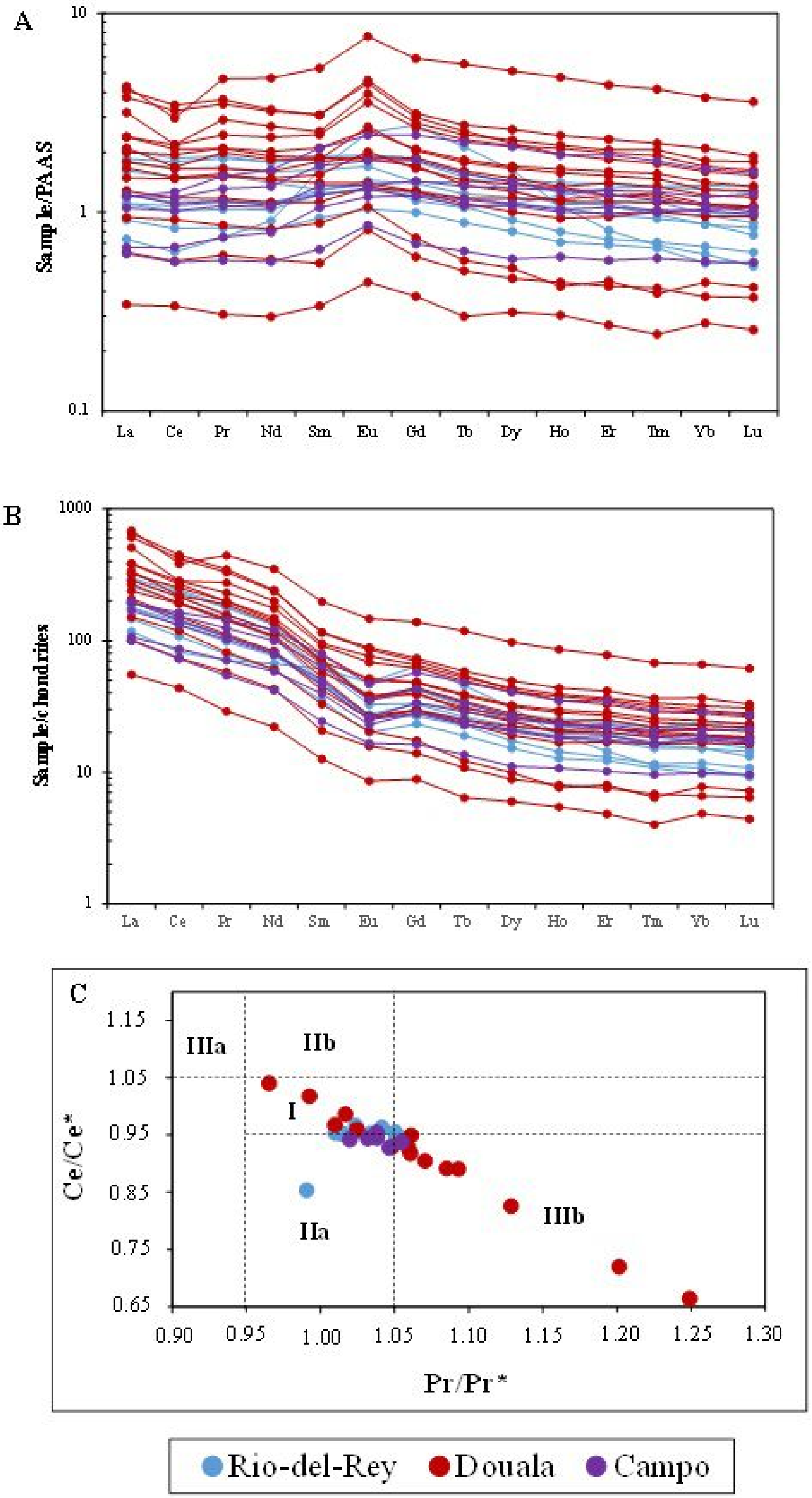

Figure 7

Normalized value of PAAS (A) and Chondrite (B) after McLennan (2001) and McDonough and Sun (1995) respectively; (C): PAAS normalized cross plot diagram of Ce/Ce* vs. Pr/Pr* used as a proxy for the Ce and La anomalies (modified after Bau et al., 1996). Notes: Field I: neither Ce nor La anomaly; Field IIa: positive La anomaly, no Ce anomaly; Field IIb: negative La anomaly, no Ce anomaly; Field IIIa: positive Ce anomaly, negative La anomaly; Field IIIb: negative Ce anomaly.

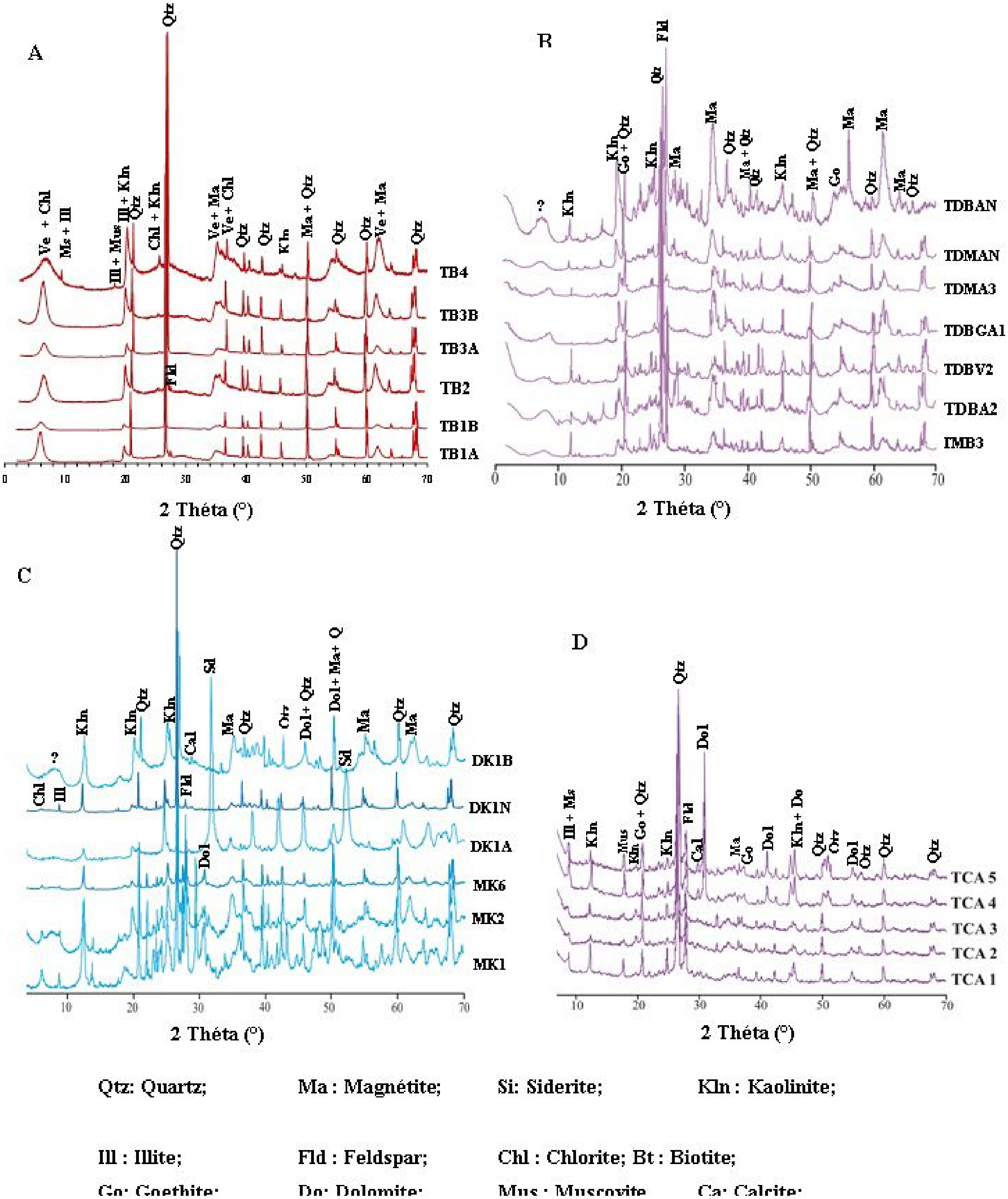

Figure 8

a: X-Ray diffraction from Douala sub-basin (southern part)

b: X-Ray diffraction from Douala sub-basin (northern part)

c: X-Ray diffraction from Rio-del-Rey sub-basin

d: X-Ray diffraction from Campo sub-basin

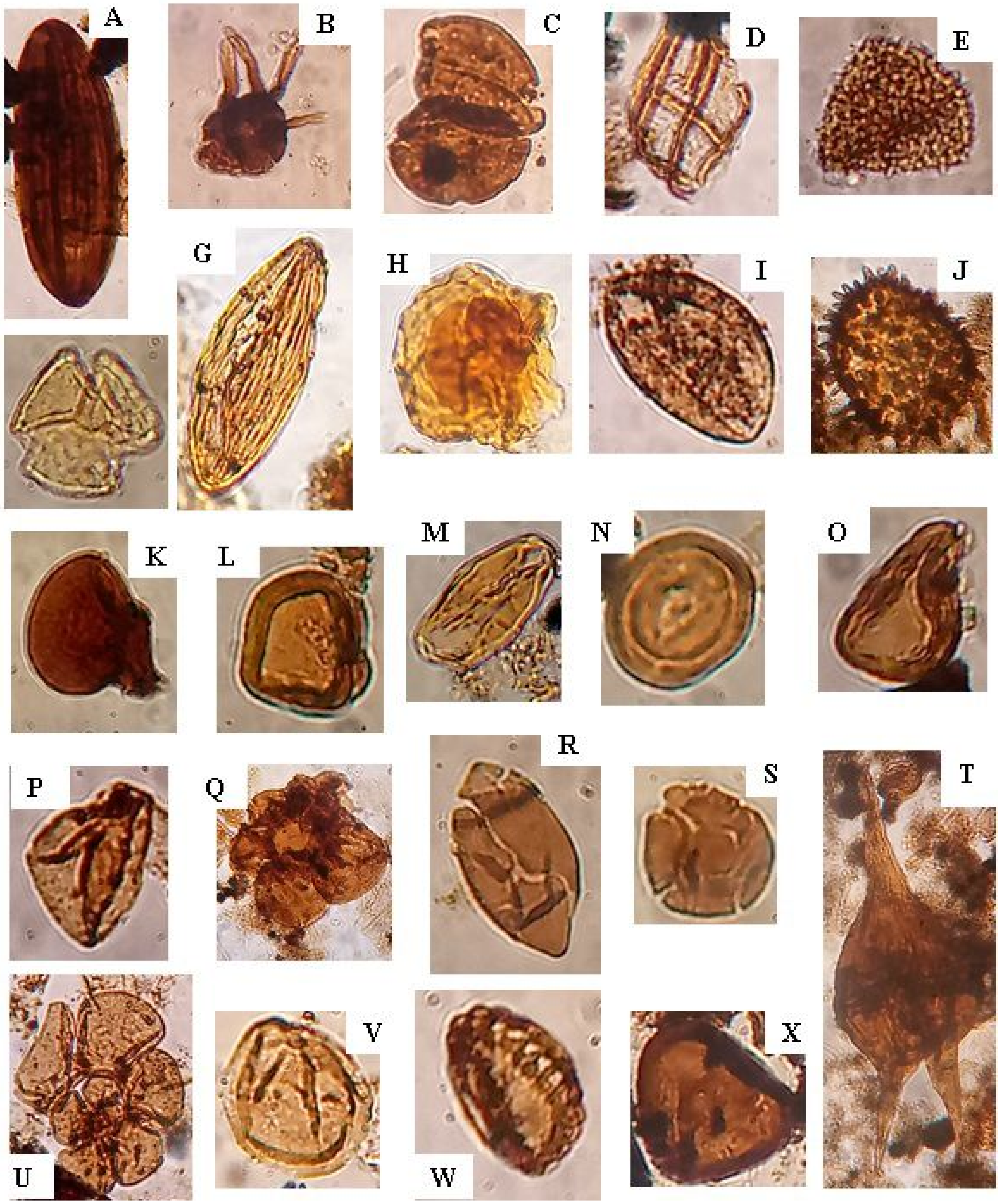

Figure 9

Palynologic content from some studied sediments: A: *Ephedripites* sp. (RDR, MK2, length=75µm); B: *Elateroplicites africaensis* (RDR, MK2, length=37.5µm); C: *Spheripollenites* sp. (RDR, MK2, length=50 µm); D: Cuticular sheet (RDR, MK2, length=40 µm); E: *Echitriporites trianguliformis* (RDR, DK1B, length=25 µm); F= *Tricolpites* sp. (DL, TDMAN2, length=25 µm); G: *Ephedripites multicostatus* (DL, TDBAN1, length=62.5

µm); H: *Crybelosporites panuceus* (DL, TDBAN1, length=57.5 µm); I: *Monocolpate* sp. (RDR, DK1B, length=37.5 µm); J: *Spinizonocolpites baculatus* (RDR, DK1B, length=62,5 µm); K: Microforaminifera ligning debris (DL, TDMAN2, length= 35 µm); L: Pollen? (CP, TC2, length= 25 µm); M: *Eucommiidites troedssnii* (CP, TC2, length=37.5); N: *Classopollis* sp. (CP, TC3, length=32.5 µm); O: *Deltoidospora* sp. (CP, TC3, length=45 µm); P: Granulate spore (DL, TDMAN2, length=30 µm); Q: Microforaminifera ligning (DL, TDMAN2, length=62.5 µm); R: Unicellular fungi (DL, TDBAN1, length=32.5 µm); S: Microforaminifaral lining (DL, TDMAN2, length=25 µm); T: *Cerodinium* sp. (RDR, DK1B, length=87.5 µm); U: Microforaminiferal ligning (DL, TDBAN1, length=67.5 µm); V: Araucariacites sp. (RDR, MK2, length=27.5 µm): W: (?) Erdtmanipollis sp. (RDR, DK1B, length=25 µm); X: Spore? (RDR, MK2, length=30 µm). N.B.: RDR= Rio del Rey sub-basin; DL= Douala sub-basin; CP= Campo sub-basin.

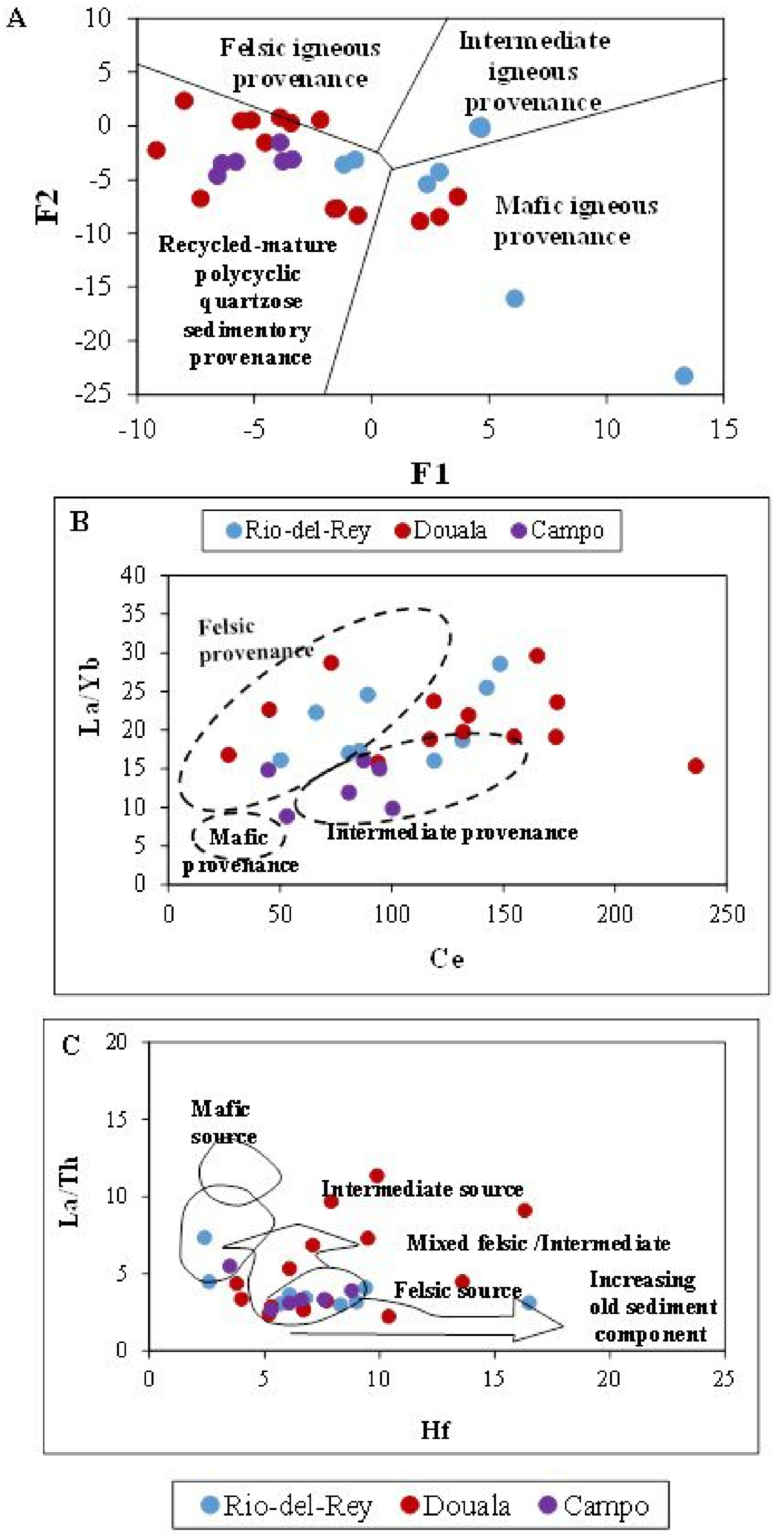

Figure 10

(A) Provenance discriminant function plot (after Roser and Korsch, 1988), (B) Ce vs. La/Yb (after Rao et al., 2011) and (C) La/Th vs. Hf (after Floyd and Leveridge, 1987) Scatter plots of provenance for the studied samples.

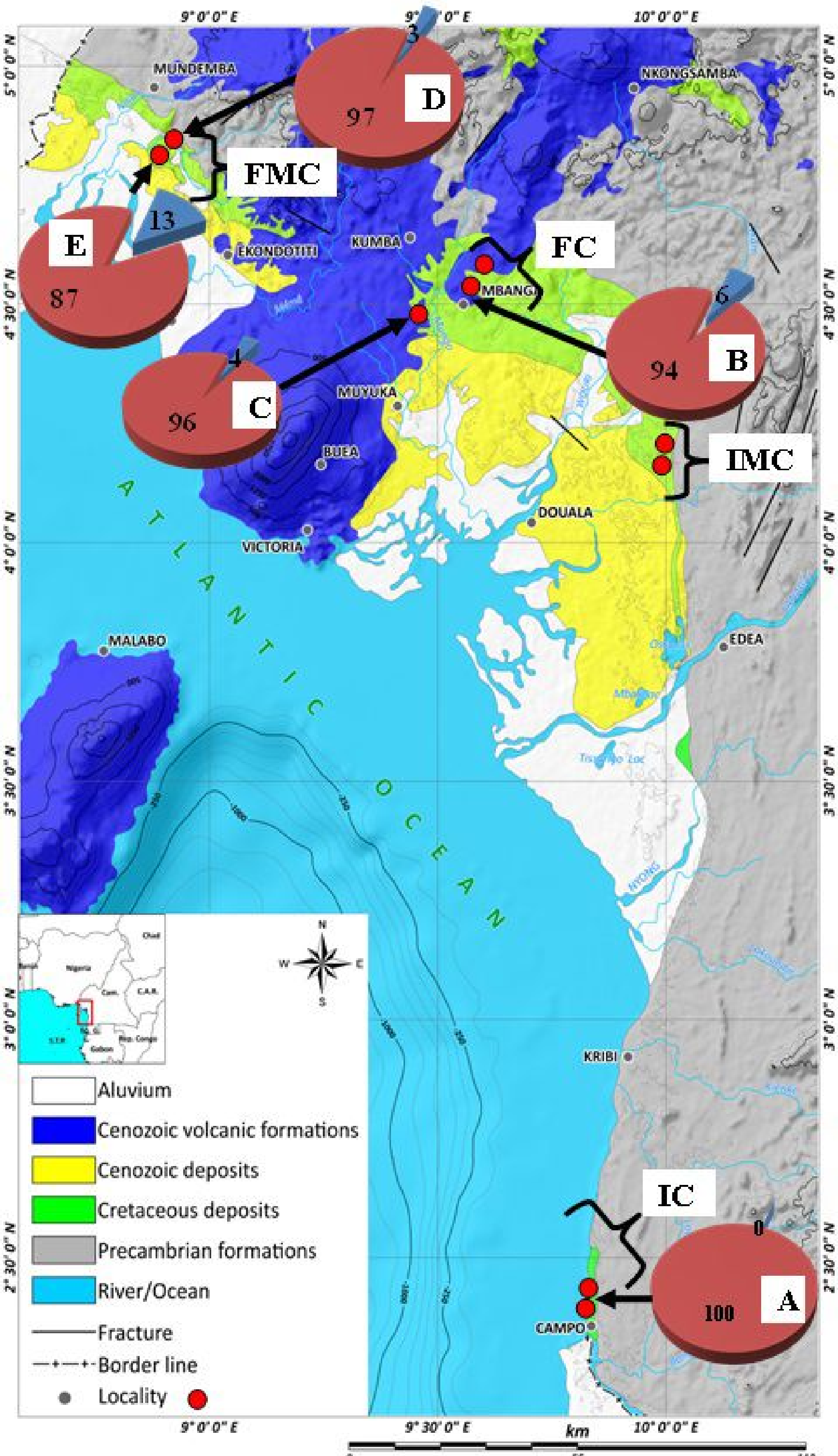

Figure 11

Location and Circular diagrams of rate of marine and non-marine palynomorphs and provenance source rocks in the studied areas; (**A**) Campo sub-basin (Barremian-Albian); (**B**) Douala sub-basin, Mbanga (Albian-Cenomanian); (**C**) Douala sub-basin, Ediki (Albian-Cenomanian); (**D**) Rio-del-Rey sub-basin (Albian-Cenomanian); (**E**) Rio-del-Rey sub-basin (Campanian-Maastrichtian); **IC** = Intermediate composition; **IMC**= Intermediate and mafic composition; **FC**= Felsic composition; **FMC**= Felsic and mafic composition. N.B.: Red color = Continental species rate; Blue color = Marine species rate.

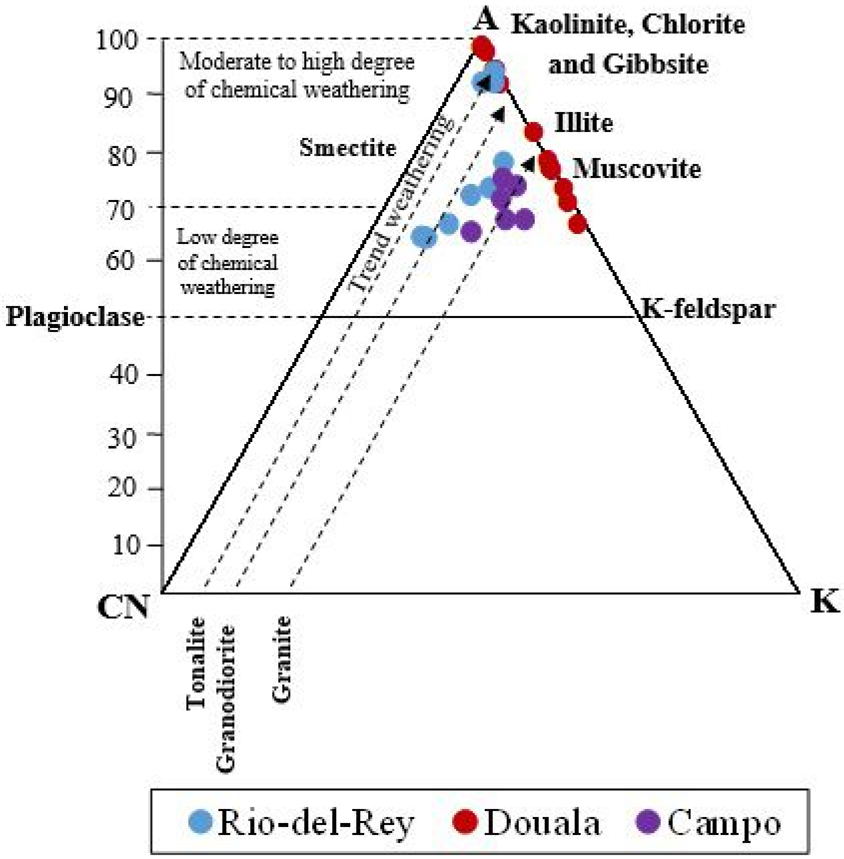

Figure 12

A-CN-K plots (after Nesbitt and Young, 1984) for the studied samples. The dotted line represents the possible weathering trend of the source rock if no K-addition is involved. The heavy solid line represents a possible weathering trend combined with K-metasomatism from the source rock.

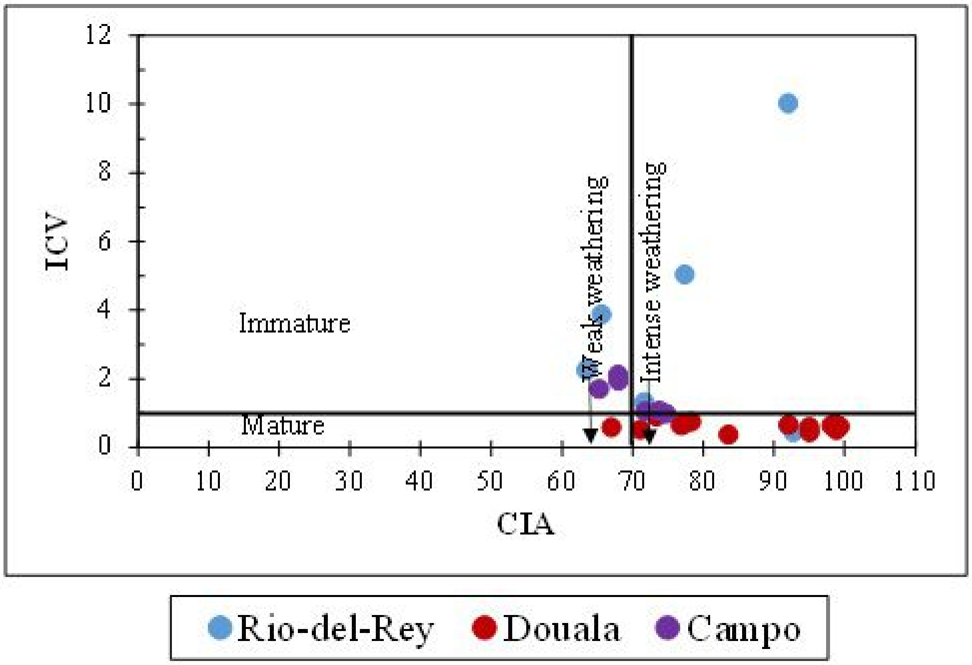

Figure 13

ICV versus CIA diagram (Nesbitt and Young 1984; Cox et al. 1995) showing the maturity of studied deposits

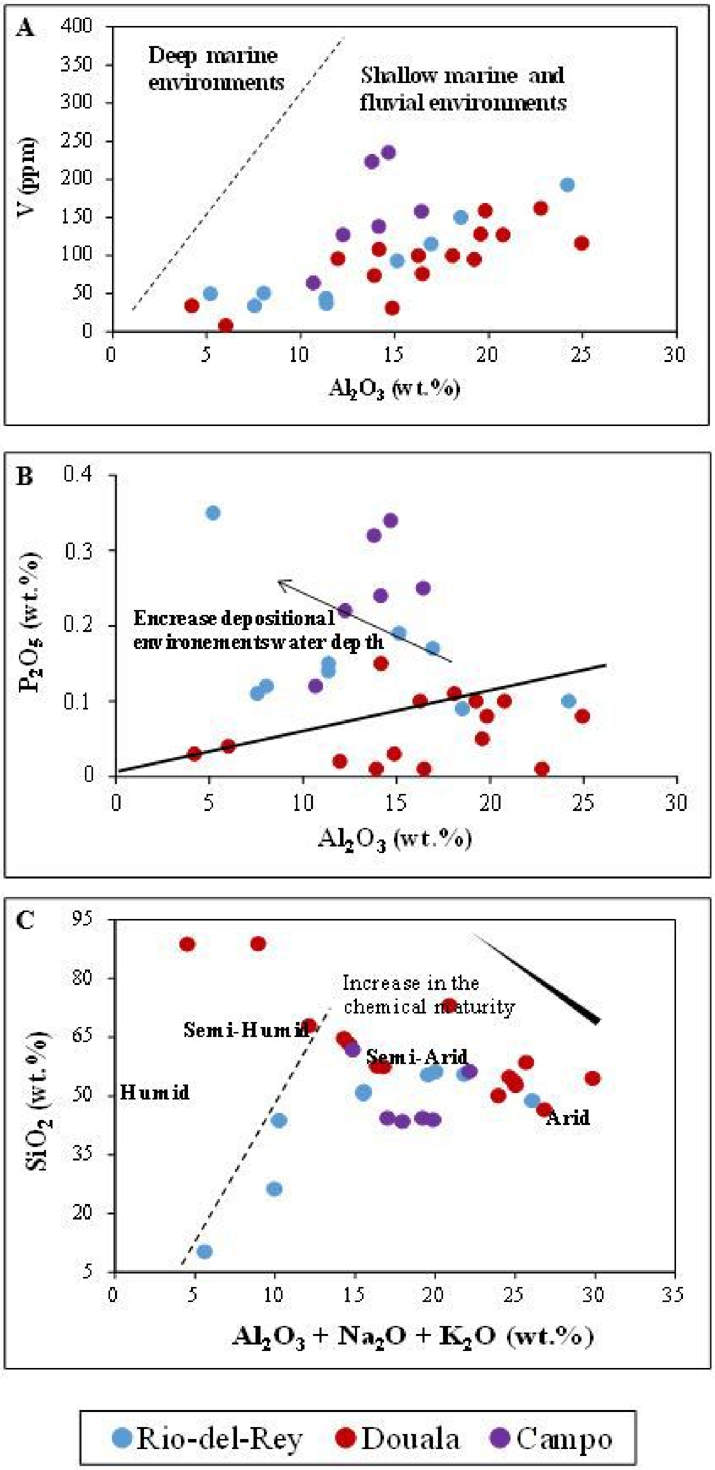

Figure 14

(A) V vs. Al_2O_3 and (B) P_2O_5 vs. Al_2O_3 plots for paleoenvironmental reconstructions (after (Mortazavi et al. 2014; Anaya-Gregorio et al. 2018), and (c) SiO_2 vs. $Al_2O_3 + K_2O + Na_2O$ plot for climate during the deposition (After Suttner and Dutta, 1986).

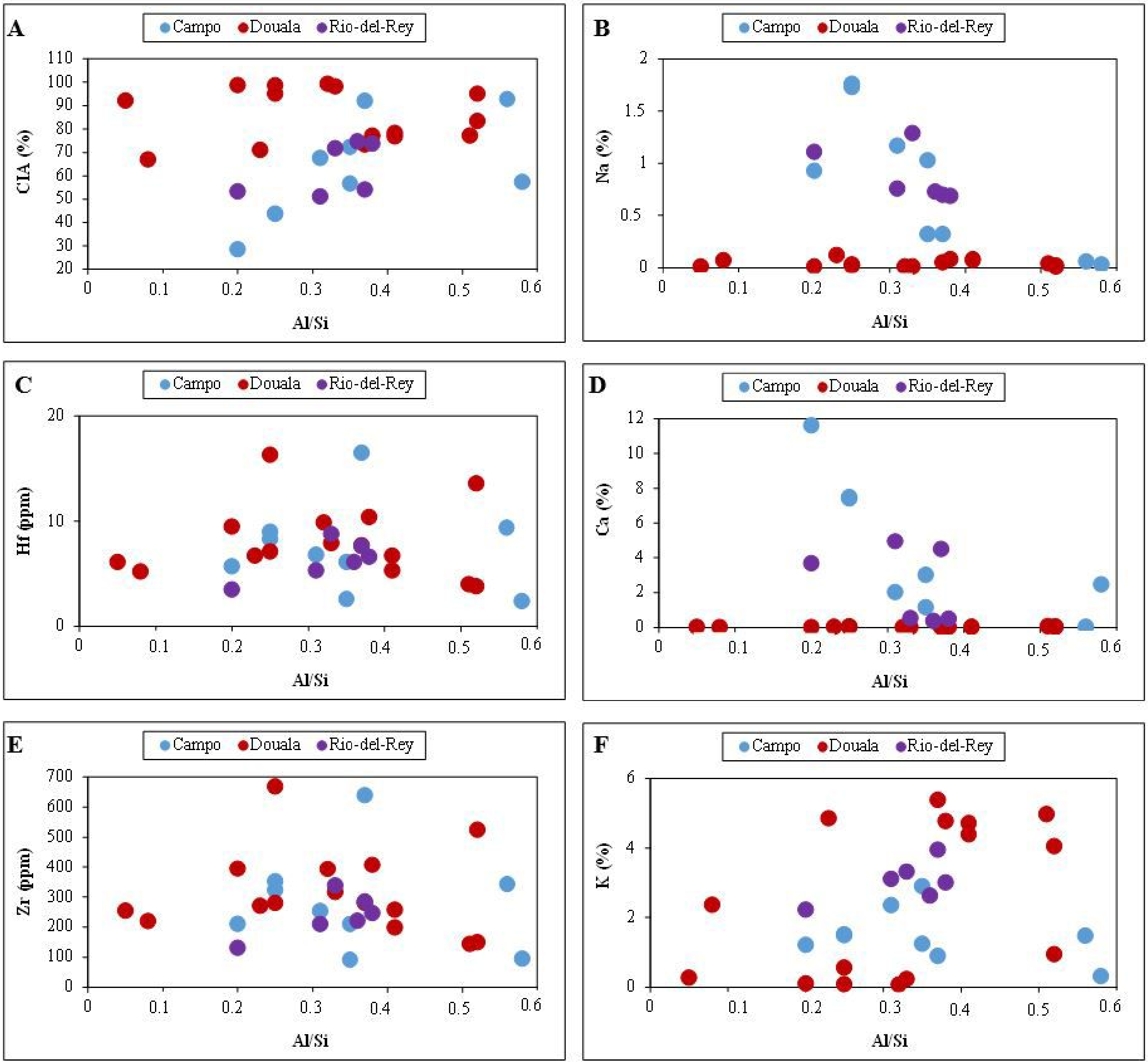

Figure 15

Plots of CIA versus Al/ Si (A), Na versus Al/ Si (B), Hf versus Al/ Si (C), Ca versus Al/ Si (D), Zr versus Al/ Si (E), K versus Al/ Si (F) to illustrate the effect of grain-size on CIA, Na, Hf, Ca, Zr, and K.

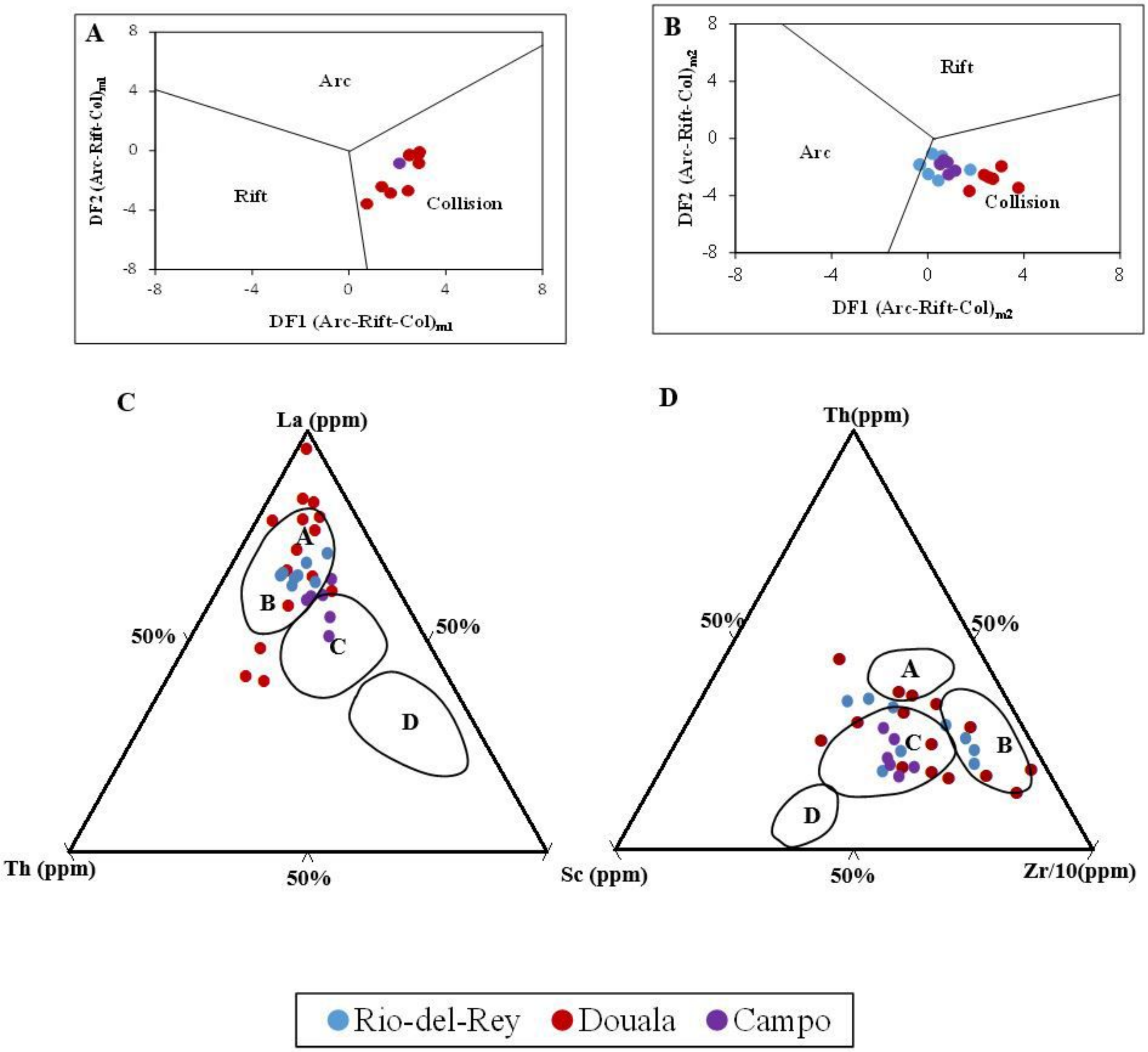

Figure 16

(**A**) Discriminant-function multi-dimensional diagram for high-silica clastic sediments (Verma and Armstrong-Altrin, 2013). The subscript m1 in DF1 and DF2 represents the high-silica diagram based on $\log_e$-ratios of major-elements. The discriminant function equations are DF1 (Arc-Rift-Col)m1 = (−0.263 × ln(TiO_2/SiO_2)adj) + (0.604 × ln(Al_2O_3/SiO_2)adj) + (−1.725 × ln(Fe_2O_3 t /SiO2)adj) + (0.660 × ln(MnO/SiO2)adj) + (2.191 × ln(MgO/SiO_2)adj) + (0.144 × ln(CaO/SiO_2)adj) + (−1.304 × ln(Na_2O/SiO_2)adj) + (0.054 × ln (K_2O/SiO_2)adj) + (−0.330 × ln(P_2O_5/SiO_2)adj) + 1.588; DF2 (Arc-Rift-Col)m1 = (−1.196 × ln(TiO_2/SiO_2)adj) + (1.604 × ln(Al_2O_3/SiO_2)adj) + (0.303 × ln(Fe_2O_3 t /SiO_2)adj) + (0.436 × ln(MnO/SiO_2)adj) + (0.838 × ln(MgO/SiO_2)adj) + (−0.407 × ln(CaO/SiO_2)adj) + (1.021 × ln(Na_2O/SiO_2) adj) + (−1.706 × ln(K_2O/SiO_2)adj) + (−0.126 × ln(P_2O_5/SiO_2)adj) - 1.068. (**B**) Discriminant-function multi-dimensional diagram for low-silica clastic sediments. The subscript m_2 in DF1 and DF2 represents the low silica diagram based on $\log_e$-ratios of major-elements. The discriminant function equations are DF1(Arc-Rift-Col)m_2 = (0.608 x ln(TiO_2/SiO_2))adj + (-1.854 x ln(Al_2O_3/SiO_2))adj + (0.299 x ln(Fe_2O_3/SiO_2))adj + (-0.550 x ln(MnO/SiO_2))adj + (0.120 x ln(MgO/SiO_2))adj + (0.194 x ln(CaO/SiO_2))adj + (-1.510 x ln(Na_2O/SiO_2))adj + (1.941 x ln(K_2O/SiO_2))adj + (0.003x ln(P_2O_5/SiO_2))adj - 0.294; DF2(Arc-Rift-Col)m_2 = (-0.554 x ln(TiO_2/SiO_2))adj + (-0.995 x ln(Al_2O_3/SiO_2))adj + (1.765 x ln(Fe_2O_3/SiO_2))adj + (-1.391 x ln(MnO/SiO_2))adj + (-1.034 x ln(MgO/SiO_2))adj + (0.225 x ln(CaO/SiO_2))adj + (0.713 x ln(Na_2O/SiO_2))adj + (0.330 x ln(K_2O/SiO_2))adj + (-0.637 x ln(P_2O_5/SiO_2))adj – 3.631. (**C**) La-Th-Sc and (**D**) Th-Sc-Zr/10 ternary diagrams (Bhatia and Crook, 1986).

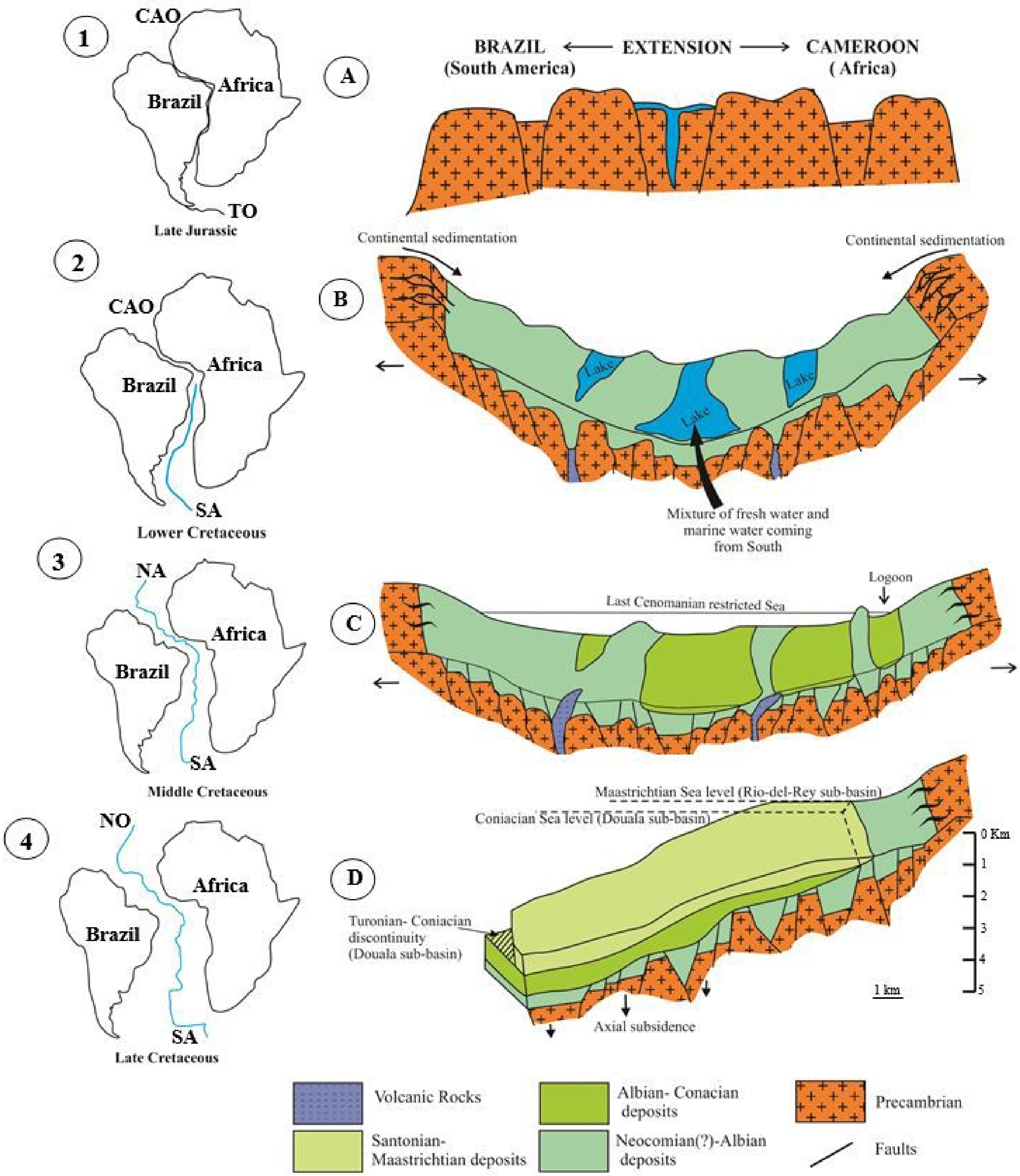

Figure 17

General paleogeographic situation of Atlantic Basin during the Cretaceous (1, 2, 3 and 4: Paleogeographic evolution between Brazil and Africa (modified from Scotese, 2001); A, B, C and D: Paleogeographic evolution of the Cameroon Atlantic Basin (modified after Njike Ngaha, 1984; Tchouatcha, 2005; Njike Ngaha et al., 2014). CAO: Central Atlantic Ocean; TO: Tethys Ocean; SA: South Atlantic; NA: North Atlantic

Supplementary Files

This is a list of supplementary files associated with this preprint. Click to download.

- Tables.docx